EARTH SCIENCES
RESEARCH JOURNAL
Earth Sci. Res. J. Vol. 28, No. 3 (September, 2024): 325 - 348

UNIVERSIDAD NACIONAL DE COLOMBIA

GEOLOGICAL ENGINEERING

A Comparative of Frequency Ratio Method, Weight of Evidence, and Analytical Hierarchy Process for Landslide Susceptibility Assessment in the Main Boundary Thrust (MBT) Region in Ranitar-Belarang Section of Udayapur District, Koshi Province, Nepal

Kabi Raj Paudyal*, Rupendra Maharjan, Birat Shrestha, and Neelam Maharjan
Central Department of Geology, Tribhuvan University, Kirtipur, Kathmandu, Nepal
* Corresponding author: kabiraj.paudyal@cdgl.tu.edu.np

ABSTRACT

A landslide susceptibility map indicates those locations which are prone to the landslide depending upon the factors that causes landslide (slope, soil type, impact of flow, etc.). This study assesses the outcomes of a landslide susceptibility analysis employing Frequency Ratios (FR), Weight of Evidence (WoE) and Analytical Hierarchy Process (AHP) in the Ranitar - Belarang region, situated in Udayapur District, Koshi province of eastern Nepal. Geologically, the region falls within the region of the Main Boundary Thrust (MBT). Google Earth imagery (CNES/Airbus and Maxar Technologies) with a spatial resolution of 20 m was utilized for landslide detection. The inventory of landslides was employed to create data sets for training and testing. Thirteen causative parameters (Slope, Distance to Thrust, Landuse, Geology, Distance to stream, Curvature, Aspect, Relief, Distance to Road, Topographic Wetness Index, Sediment Transport Index, Sediment Power Index, Rainfall), derived from topographic, geological, and land-use maps were considered in the analysis. The AHP ratings were assigned based on the expert judgment whereas, the FR and WoE ratings were computed based on these causative factors and training events. Subsequently, a landslide susceptibility map was generated by amalgamating causative factors that yielded FR, AHP, and WoE scores with validation using the AUC- ROC curve resulting in an 86.4%, 68.5%, and 89.9% accuracy respectively. Among the three methods of analysis, Weight of Evidence (WoE) has the highest accuracy (89.9%) in predicting landslides followed by Frequency Ratio (86.4%). Also, it was found that distance from the Main Boundary Thrust (MBT), land use, relief, and distance from the road emerged as the most influential factors contributing to landslide occurrence.

Keywords: Landslide Susceptibility, Main Boundary Thrust (MBT), Frequency Ratios (FR), Weight of Evidence (WoE), Analytical Hierarchy Process (AHP), Nepal

Comparación de los métodos de Relación de Frecuencia, Análisis de la Evidencia y Proceso de Jerarquía Analítica para la evaluación de la susceptibilidad a deslizamientos de tierra en la falla de empuje frontal del Himalaya en la sección Ranitar-Belarang, distrito de Udayapur, provincia de Koshi, Nepal

RESUMEN

Un mapa de susceptibilidad de deslizamientos de tierra indica aquellos puntos que son propensos a los deslizamientos de acuerdo con los factores que lo causan (pendiente, tipo de suelo, impacto de la circulación de aguas, etc.). Este estudio evalúa los resultados de los análisis de susceptibilidad de deslizamientos preparados con los modelos Relación de Frecuencia, Análisis de la Evidencia y Proceso de Jerarquía Analítica, en la región de Ranitar-Belarang, situada en el distrito de Udaipur, provincia oriental de Koshi, Nepal. Geológicamente, la región se ubica en la falla conocida como empuje frontal del Himalaya. Se utilizaron imágenes de Google Earth (Tecnologías CNES/Airbus y Maxar), con una resolución espacial de 20 m, para detectar deslizamientos de tierra. El inventario de deslizamientos se empleó para crear grupos de datos de entrenamiento y prueba. En este análisis se consideraron trece parámetros causantes (pendiente, distancia al cabalgamiento, uso del suelo, geología, distancia a la corriente, curvatura, aspecto, relieve, distancia a caminos, Índice de Humedad Topográfica, Índice de Transporte de Sedimentos, Índice de Potencia de Sedimentos, y lluvia), derivados de mapas topográficos, geológicos, y de uso del suelo. Los criterios del Proceso de Jerarquía Analítica se asignaron con base a un juzgamiento experto, mientras que los criterios de la Relación de Frecuencia y Análisis de la Evidencia se computaron de acuerdo con los factores causativos y los eventos de entrenamiento. Seguidamente se generó un mapa de susceptibilidad de deslizamientos al converger los factores causativos de los modelos Relación de Frecuencia, Proceso de Jerarquía Analítica, y Análisis de la Evidencia, con una validación ejecutada con el método Área bajo la curva ROC (Característica Operativa del Receptor), la cual calculó una precisión de 86.4 %, 68.5%, y 89.9, respectivamente. Dentro de estos tres métodos, el Análisis de la Evidencia tiene el mayor índice de precisión (89.9 %) en la predicción de deslizamientos, seguido por la Relación de Frecuencia (86.4 %). Además, se encontró que la distancia a la falla de empuje frontal del Himalaya, el uso del suelo, relieve y distancia a caminos son los factores más influyentes en la ocurrencia de deslizamientos.

Palabras Claves: Palabras clave: Susceptibilidad de deslizamientos; falla empuje frontal del Himalaya; Relación de Frecuencia; Análisis de la Evidencia; Proceso de Jerarquía Analítica; Nepal.

Record
Manuscript received: 31/01/2024
Accepted for publication: 18/10/2024

How to cite item:
Paudyal, K. R., Maharjan, R., Shrestha, B., & Maharjan, N. (2024). A Comparative of Frequency Ratio Method, Weight of Evidence, and Analytical Hierarchy Process for Landslide Susceptibility Assessment in the Main Boundary Thrust (MBT) Region in Ranitar-Belarang Section of Udayapur District, Koshi Province, Nepal. *Earth Sciences Research Journal, 28*(3), 325-348 https://doi.org/10.15446/esrj.v28n3.112740

1. Introduction:

Landslides are a major concern in Nepal's mountainous regions, causing environmental damage and endangering lives. The geomorphic and tectonic evolution of the Nepal Himalayas plays a pivotal role in the formation of deep and steep river valleys in central and eastern Nepal (Hasegawa et al., 2008). These valleys are notably prone to a myriad of large and small-scale landslides. Nepal has been heavily affected by landslides in recent years, with substantial loss of life, property damage, and economic impact (Bhandari et al., 2024). Creating accurate landslide susceptibility maps is crucial for disaster prevention and mitigation efforts. These maps identify areas with a higher likelihood of landslides, allowing authorities to take proactive measures to protect people and infrastructure. Despite existing research on landslide modeling in Nepal, there's a need for further studies that compare the effectiveness of different mapping techniques. The present study area Ranitar - Belarang faces multiple challenges related to slope instabilities, primarily attributed to its steep terrain, rugged landscape, the presence of the thrust (MBT), and the precarious condition of the rock formations. This section of Nepal Himalaya has not been studied in terms of landslide susceptibility with special reference to the Main Boundary Thrust (MBT), a master thrust of the Himalaya, as a cause of landslides in Nepal. Different contributing factors like topography, lithology, rainfall intensity, vegetation condition, lineaments facilitate activation and reactivation of landslide events. Various researchers have developed different techniques for landslide susceptibility mapping, including statistical methods and machine learning approaches. Due to the simplicity, accessibility, and reliability in producing accurate susceptibility maps, two statistical methods; weight of evidence, and frequency ratio, and multi criteria decision making approach, analytical hierarchy process are chosen for the study and compared with other methods.

2. Study Area

The study area, Ranitar-Belarang, is situated in Udayapur district in eastern Nepal, as depicted in Figure 1. The research site spans an altitude range of 120 meters to 1000 meters, covering a total area of 89.76 sq. km. The geographical coordinates of the study area are defined by a longitude range of 86.969431° to 87.184146° and a latitude range of 26.926310° to 26.852557 °. The geology of the study area is divided into five major geological groups: Phongaswa, Barahakshetra, Siwalik Group, Gondwana Group, and Midland Group (DMG, 1984). Accessibility to the study area is facilitated within a 25-kilometer radius of Mahendra Highway through local roads, namely Dharan Chatara Barahalsetra and Jhumka (MRM) Chatara Road. Additionally, the area is connected to a network of graveled streets and footpaths, enhancing its overall transportation infrastructure.

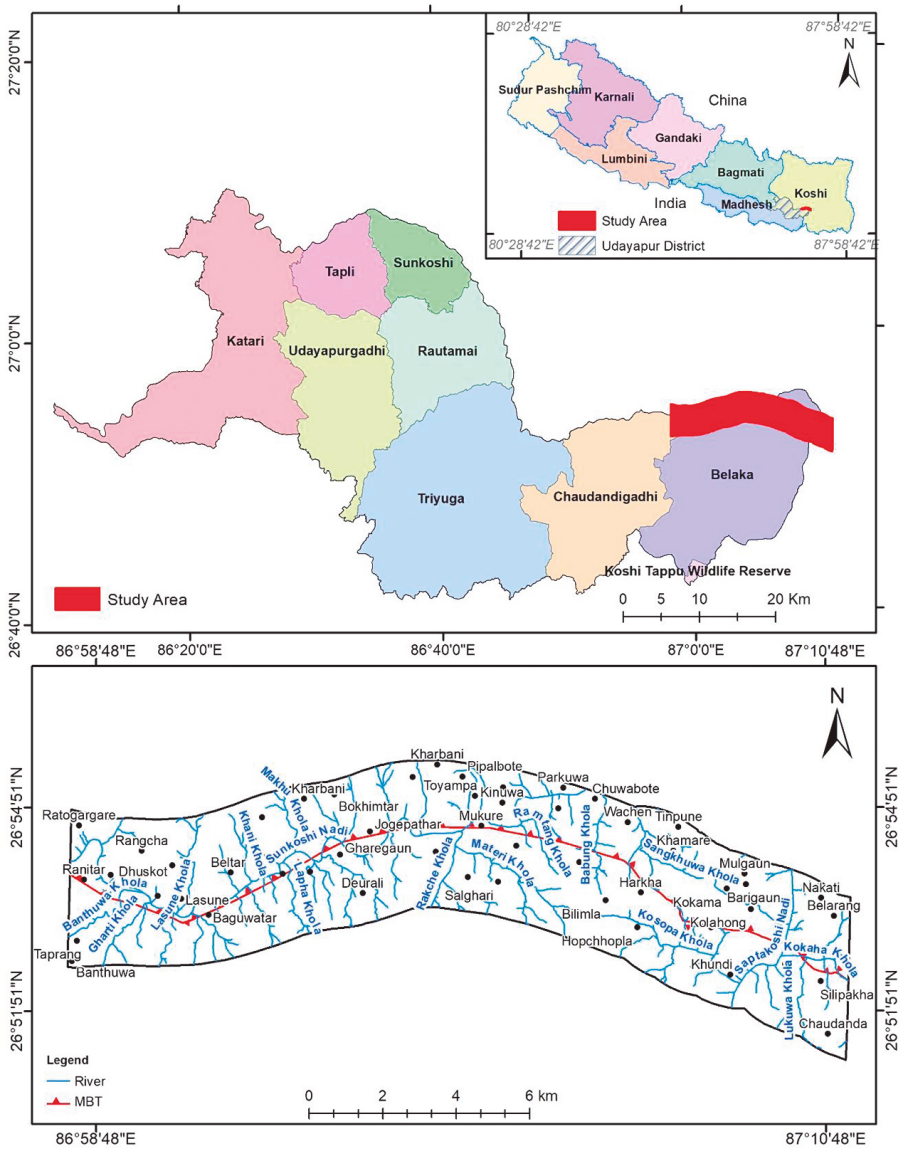

Figure 1. Location map of the Ranitar - Belarang section

3. Materials and Methods:

It is imperative to conclude that the causative factors of landslides play a pivotal role in influencing the spatial distribution of such events. The understanding that future landslides are likely to occur under conditions akin to those observed in previous incidents is crucial for effective landslide susceptibility mapping, as emphasized by (Lee & Talib, 2005).

In recent decades, numerous scholars have devised effective methodologies for constructing accurate landslide susceptibility maps. Various researchers have adopted different methods for landslide susceptibility in Nepal Himalaya such as frequency ratio (Thapa & Bhandari, 2019; Bhandari et al., 2024, Goetz et al., 2015; Hong et al., 2016; M. J. Lee et al., 2016), Analytical Hierarchy Process (Pathak et al., 2021; Pourghasemi et al., 2012; T. L. Saaty, 2004), Weight of Evidence (Dahal et al., 2008; Gómez & Kavzoglu, 2005, Pokharel & Bhandari, 2019) logistic regression (Chen et al., 2017; Steger et al., 2016), Budha et al, 2016 and 2020, decision trees (S. Lee & Park, 2013; Pradhan, 2013; Tsangaratos & Ilia, 2016), fuzzy logic (Feizizadeh et al., 2014; Park et al., 2014; Pradhan, 2011), neuro fuzzy systems (Aghdam et al., 2016; M.-J. Lee et al., 2015; Pradhan, 2013), support vector machines (S. Lee et al., 2017; Peng et al., 2014; Pradhan, 2013; Tien Bui et al., 2017), artificial neural networks (Conforti et al., 2014; Pradhan & Lee, 2010; Tsangaratos & Benardos, 2014), and a multimethod approach (Althuwaynee et al., 2016; Pham et al., 2016; Pradhan, 2010; Yalcin et al., 2011), have been developed. AHP offers a systematic approach to decision-making by breaking down complex problems into a hierarchy of simpler sub-problems. This structured approach is not typically available in methods like fuzzy logic or neurofuzzy systems, which can be more abstract and less intuitive. WoE provides a clear and intuitive understanding of the relationship between causative factors and landslide occurrence, which can be more accessible than the complex interpretations required for machine learning models like SVM or ANN. FR is straightforward to implement and understand, making it accessible for researchers with limited resources or expertise. This simplicity is a significant advantage over more complex methods like neurofuzzy systems or SVM, which require extensive parameter tuning and computational resources.

Among various models, this paper assesses the effectiveness of the landslide susceptibility study using three methods viz. Analytical Hierarchy Process (AHP), Weight of Evidence (WoE), and Frequency Ratio (FR). These models offer the advantage of ranking causative variables based on their likelihood of causing a landslide. Additionally, it enables the determination of whether a given set of causative factor values would pose a hazard in the event of a landslide, as noted by (Kannan et al., 2013). The overall methodological scheme adopted for the present study plan is shown in Figure 2.

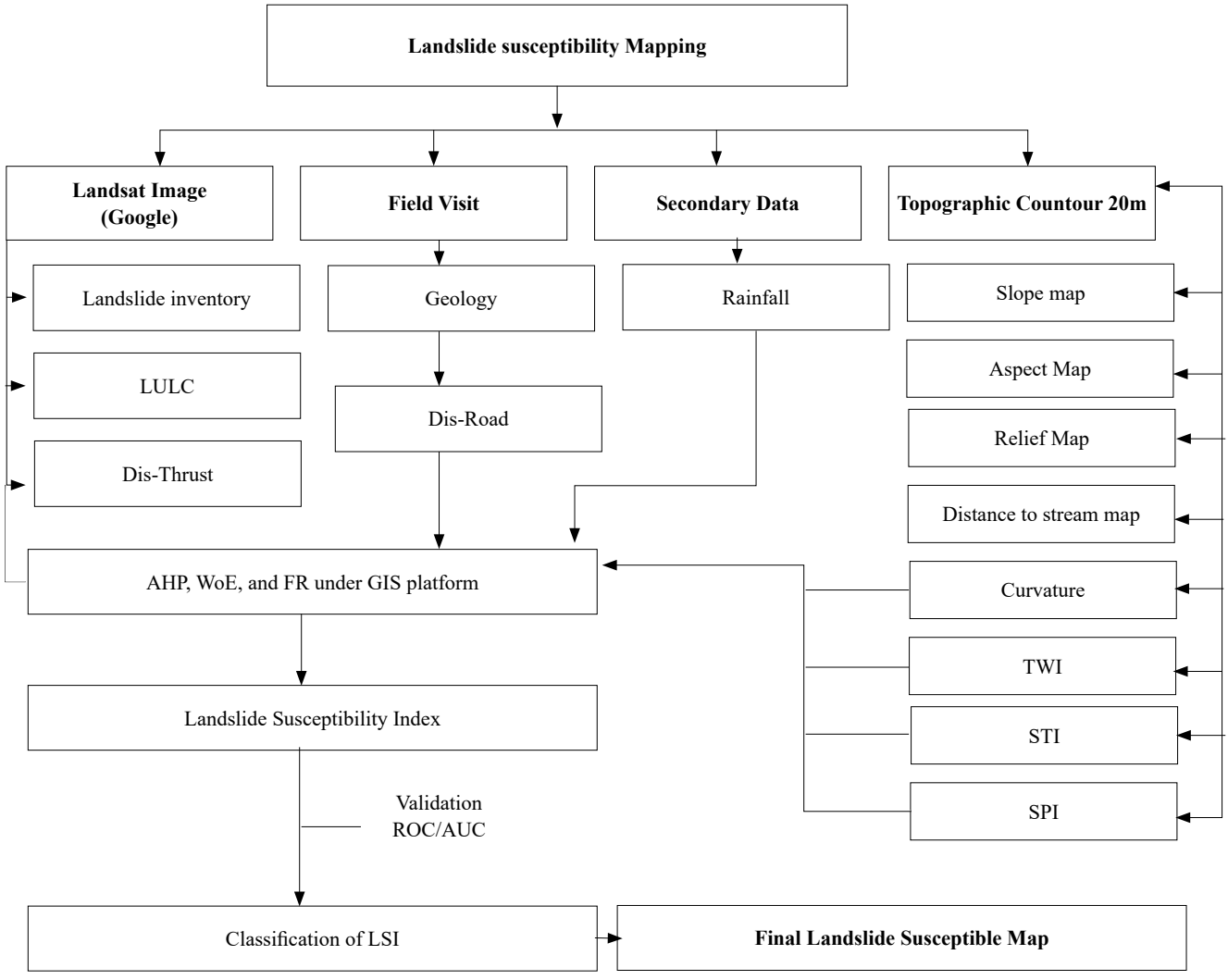

Figure 2. Methodology used in analysis of landslide susceptibility mapping using FR method.

The landslide inventory consisting of 120 landslides, was prepared through the manual digitization of aerial photographs / satellite images obtained from Google Earth (March 2020) and divided into training samples (70%, n=84) and testing samples (30%, n=36). The Landslide Susceptibility Index (LSI) model was then developed utilizing the training sample, and its validation was carried out using the testing sample through ROC-AUC analysis in SPSS (Figure 2).

Landslide susceptibility mapping involves the generation of thematic data layers, as emphasized by (Camarinha et al., 2014). Consequently, thirteen thematic layers were incorporated into a 20 m × 20 m cell grid, encompassing geology, slope, aspect, curvature, distance from the stream, distance from the road, distance from the thrust (MBT), relief, land use land cover, rainfall, topographic wetness index, stream power index and sediment transport index.

To derive topographic and hydrologic parameters, a Digital Elevation Model (DEM) was utilized, derived from a Triangulated Irregular Network (TIN) surface. This TIN was constructed using ArcMap 10.4.1 and contour lines extracted from digitized topographic maps at 20 m intervals. Various topographic and hydrologic characteristics including slope gradient, curvature, slope aspect, relief, distance from the stream, were considered for landslide susceptibility analysis.

The Land Use Land Cover (LULC) map was created using ArcMap 10.4.1 by digitizing the image. Geological information and the location of the thrust (MBT) were derived from data obtained from the petroleum block (Department of Mines and Geology, Government of Nepal) and verified during the present field visit. The Euclidean distance algorithm was employed to generate the MBT distance map. This comprehensive approach ensures a multi-dimensional analysis incorporating geological, topographic, and land cover factors for an accurate landslide susceptibility assessment.

The landslide inventory map was employed to intersect with all-factor maps, leading to the generation of tabulated data after the preparation of thirteen factor maps. The landslide susceptibility was mapped using the frequency ratio, weight of evidence and analytical hierarchy methods. The resulting LSI map was categorized into three zones: stable, quasi-stable, and unstable zones. These zones are categorized on the basis of the histogram curve obtained from sensitivity versus 1-specificity. Larger values of the test result variable indicate stronger evidence for a positive actual state. The classification was based on the LSI values obtained from the Frequency Ratio (FR), Weight of Evidence (WoE), and Analytical Hierarchy Process (AHP) methods. This ensures that the classification is not biased by subjective opinions or personal judgments. The classification method takes into account the spatial relationships between the cells, ensuring that the classification is not only based on the LSI values but also on the spatial context.

Frequency Ratio Method:

To evaluate the likelihood of landslides, it is crucial to comprehend the specific physical characteristics of the area and the processes that contribute to landslide occurrence. The frequency ratio emerges as a quantitative technique for assessing landslide susceptibility by leveraging Geographic Information System (GIS) and spatial data (Bonham-Carter, 1994; Chen, Chai, et al., 2016; Chen, Wang, et al., 2016; Ding et al., 2017; S. Lee & Talib, 2005). Widely acknowledged and effectively applied in landslide susceptibility mapping, the frequency ratio (FR) method establishes a quantified relationship between the landslide inventory and the causative factors (Chen, Chai, et al., 2016; Reis et al., 2012; Umar et al., 2014; Q. Wang & Li, 2017; Wu et al., 2016; Yilmaz, 2009;(Thapa & Bhandari, 2019).

This technique, as outlined in Eq. (1), involves the amalgamation of the landslide inventory map and the factor map to compute the frequency ratio (FR) for each class of the causative factors (Fayez et al., 2018; Mondal & Maiti, 2013).

$$FR = \frac{Npix\,(1)/Npix\,(2)}{\sum Npix\,(3)/\sum Npix\,(4)} \quad (1)$$

Where Npix(1) = The number of pixels containing Landslide in a class
Npix(2) = Total number of pixels of each class in whole area.
Npix(3) = Total number of pixels containing landslide.
Npix(4) = Total number of pixels in the study area.

The derived frequency ratio is aggregated to formulate a Landslide Susceptibility Index (LSI) map using Eq. (2) (S. Lee & Talib, 2005).

$$LSI = FR_1 + FR_2 + FR_3 + FR_4 + \ldots\ldots\ldots + FR_n \quad (2)$$

Landslide Susceptibility Index map (LSI) was prepared by combining all thirteen factor maps (Figure 19 & Figure 21).

$$Final\ LSI = PR_{d1} * FR_1 + PR_{d2} * FR_2 + PR_{d3} * FR_3 + PR_{d4} * FR_4 + \ldots\ldots\ldots + PR_{dn} * FR_n$$

Where,
PR = Predictive ratio of each domain.
FR = Frequency ratio of each class of a domain.
Here the predictive ratio (Table 3) is the weight given to the domain from table-1 which is calculated as in eq.3 below:

$$PR = (Max\ RF - Min\ RF)/(Min\ RF\ of\ Max\ RF - Min\ RF) \quad (3)$$

Where RF stands for relative frequency. It is the ratio of FR of a class of a domain to total FR of the domain.

Analytical Hierarchy Process (AHP):

The acronym AHP refers to the Analytical Hierarchy Process, alternatively recognized as Multi-Criteria Decision Making (MCDM). Originating in the 1970s, it was conceived by Thomas L. Saaty, who collaborated with Ernest Forman to create Expert Choice in 1983 (T. Saaty, 1980). Since its inception, AHP has undergone thorough examination and refinement. This method provides a precise approach to assigning weights to decision criteria. The strength of AHP methods depends upon the consistency index that determines the consistency of decision in solving the multi-criteria parameters thus reducing bias in decision making (Abusarhan, 2011). It involves leveraging the expertise of individual contributors to gauge the relative significance of factors through pairwise comparisons. Each respondent is tasked with evaluating the relative importance between two items using a specially designed questionnaire. However, the detail information about the field knowledge around the study area of the researcher plays a vital role to assign weightage of different parameters.

Pairwise comparison matrix is created with the help of scale of relative importance viz.

- 1. ▼ Equal Importance
- 3. ▼ Moderate Importance
- 5. ▼ Strong Importance
- 6. ▼ Very Strong Importance
- 9. ▼ Extreme Importance

Note: 2, 4, 6 & 8 are Intermediate Values 1/3, 1/5, 1/7, 1/9 are values for inverse comparison.

Generally, three steps are considered during the AHP calculation (Table 1). One of the key strengths of AHP is the use of pair-wise comparison to determine the precise ratio of priorities. In this study, the pair-wise comparison matrix was constructed for the identification of landslide susceptible zones. The relative important of two selected criteria were compared in the pair-wise comparison stage. The comparisons were done to complete the development of matrices. The judgment of the relative importance of two selected criteria was carried based on the experience and knowledge. The scales of 1, 3, 5, 7 and 9 were used to for the comparison in AHP as to ensure the decision is made at a higher level of confidence. The opposite diagonal value represents its reciprocal values.

Table 1. Steps involved in developing the AHP model in Ranitar - Belrang Section

Step-1. AHP - Pairwise Comparison Matrix					
Ratings	**Parameter 1**	**Parameter 2**	**Parameter 3**	**Parameter 4**	**Parameter 5**
Parameter 1	1	1/x (j,i)	1/x (j,i)	1/x (j,i)	1/x (j,i)
Parameter 2	x (i,j)	1	1/x (j,i)	1/x (j,i)	1/x (j,i)
Parameter 3	x (i,j)	x (i,j)	1	1/x (j,i)	1/x (j,i)
Parameter 4	x (i,j)	x (i,j)	x (i,j)	1	1/x (j,i)
Parameter 5	x (i,j)	x (i,j)	x (i,j)	x (i,j)	1
…	…	…	…	…	…
Sum	Y1	Y2	Y3	Y4	Y5

Step-2. Normalized- Pairwise Comparison Matrix						
Ratings	**Parameter 1**	**Parameter 2**	**Parameter 3**	**Parameter 4**	**Parameter 5**	**Criteria Weight (Wc)**
Parameter 1	xij/Y1	xij/Y2	xij/Y3	xij/Y4	xij/Y5	Wc1
Parameter 2	xij/Y1	xij/Y2	xij/Y3	xij/Y4	xij/Y5	Wc2
Parameter 3	xij/Y1	xij/Y2	xij/Y3	xij/Y4	xij/Y5	Wc3
Parameter 4	xij/Y1	xij/Y2	xij/Y3	xij/Y4	xij/Y5	Wc4
Parameter 5	xij/Y1	xij/Y2	xij/Y3	xij/Y4	xij/Y5	Wc5
…	…	…	…	…	…	…
Sum	1	1	1	1	1	1

Step. 3 Calculation for Consistency Ratio							
Ratings	**Parameter 1**	**Parameter 2**	**Parameter 3**	**Parameter 4**	**Parameter 5**	**Weighted Sum**	**Lamda Max**
Parameter 1	1*Wc1	(1/x (j,i))*Wc2	(1/x (j,i))*Wc3	(1/x (j,i))Wc4	(1/x (j,i))*Wc5	Z1	Z1/Wc1
Parameter 2	x (i,j)*Wc1	1	(1/x (j,i))*Wc3	(1/x (j,i))Wc4	(1/x (j,i))*Wc5	Z2	Z2/Wc2
Parameter 3	x (i,j)*Wc1	x (i,j)*Wc2	1	(1/x (j,i))Wc4	(1/x (j,i))*Wc5	Z3	Z3/Wc3
Parameter 4	x (i,j)*Wc1	x (i,j)*Wc2	x (i,j)*Wc3	1	(1/x (j,i))*Wc5	Z4	Z4/Wc4
Parameter 5	x (i,j)*Wc1	x (i,j)*Wc2	x (i,j)*Wc3	x (i,j)*Wc4	1	Z5	Z5/Wc5
…	…	…	…	…	…	…	…
Sum	Y1	Y2	Y3	Y4	Y5	C.I = [($Avg.\ \lambda_{max}$ - N)/(N-1)]	C.R = [$C.I$ / $R.I$]

Random Index (RI)										
N	1	2	3	4	5	6	7	8	9	10
R.I Value	0	0	0.58	0.9	1.12	1.24	1.32	1.41	1.45	1.49
Where, xij / xji = scale of relative importance, CI= Consistency Index, and DR Consistency Ratio										

The Analytical Hierarchy Process (AHP) is a method where decisions are made by assigning weights through pairwise comparisons without inconsistencies. This process involves breaking down a decision problem into factors, arranging them in a hierarchical order, assigning numerical values to indicate their importance, creating a comparison matrix, and computing a normalized principal eigenvector to determine the weight of each factor. Essentially, the success factor in AHP implementation is dependent on the skills and understanding of decision makers in particular in order to understand the elements impacting their decision. (William, 2007)

AHP is used in landslide susceptibility analysis (Figure 23) because it allows experts to include all types of information related to landslides in the decision process. The method ensures that judgment considers all available information, and discussions are structured based on experts' knowledge and experiences. When a consensus is reached, the weights for each relevant factor are automatically calculated. The method can also identify and correct inconsistencies in the decision process using consistency index values. However, a drawback of AHP is that personal preferences in ranking factors may vary among different experts.

Weight of Evidence (WoE):

The WoE method estimates whether a landslide happened or not in a specific grid cell and also evaluates the level of influence (expressed as "weight") that each variable has on the occurrence of a landslide event (Dahal et al., 2008; Gómez & Kavzoglu, 2005; Pokharel & Bhandari, 2019). This helps us understand both the occurrence and the importance of different factors in the development of landslides (Barbieri & Cambuli, 2009).

This model was initially developed for assessing mineral potential in the 1980s (Agterberg et al., 1993; Bonham-Carter, 1989, 1994; Bonham-Carter et al., 1988; Kemp et al., 2001) state that although the method was initially intended for non-spatial applications, it can also be utilized for spatial predictions when the aim is the probability of point occurrences. The WoE model relies on figuring out positive and negative weights, represented as W^+ and W^- which are assigned to various categories of causative factors. The positive and negative weights are defined as (Bonham-Carter, 1994):

$$W_i^+ = \frac{P\{Y\}}{P\{\underline{Y}\}} \quad 4)$$

$$W_i^- = \frac{P\{Y\}}{P\{\underline{Y}\}} \quad 5)$$

where, "$\log_e$ " is the natural log, X and $\underline{X}$ are the presence and absence of potential landslide contributing factor respectively, Y and $\underline{Y}$ are the presence and absence of landslide respectively. In general, the weight can be calculated by using the equation:

$$W = \left(\frac{Event\ \%}{Non-\ event\ \%}\right) \quad 6)$$

At first, in the study thirteen landslide contributing factors (slope, aspect, curvature, relief, land use, distance from road, distance from thrust, distance from stream, geology, Topographic Wetness Index, Stream Power Index and Sediment Transport Index) were considered, classified into different classes based on their values and their thematic layers were produced in GIS. The pixel percentage of the landslide and pixel percentage of the landslide contributing factors of each class and subclass were calculated. For simplicity, the equation (6) can be modified in the form of equation (7) as:

$$Weight\ (W) = log_e\left(\frac{(Npix\ of\ landslide,\%)}{(Npix\ of\ class,\%-\ Npix\ of\ landslide,\%)}\right) \quad 7)$$

Where, Npix: the number of pixels.

The derived weight of each causative factors with respect to the presence or absence of landslides were calculated. If the weight is positive, it means the factor supports the occurrence of landslides. If it's negative, then the factor does not favor landslides. Based on the calculations, weighted maps of each factor were produced, and each map were added and overlaid using the equation (8) to obtain landslide susceptibility maps.

Landslide Susceptibility Map=

$$W_{slope}+W_{aspect}+W_{curvature}+W_{relief}+W_{landuse}+W_{disroad}+W_{disthrust}+W_{disstream}+W_{geology}+W_{rainfall}+W_{TWI}+W_{SPI}+W_{STI}\cdots \quad 8)$$

Landslide susceptibility map (LSI) was prepared by combining all thirteen factor maps (Figure 25).

Landslide Inventory

Utilizing freely available Landsat images from Google Earth, in conjunction with on-site field visits, a total of 120 landslides were mapped, covering an aggregate area of 1.007 km² (refer to Figure 3). The sample image of landslide in the study area is shown in Figure 4.

Influencing Factors:

The selection criteria for these thirteen causative factors were based on their relevance to landslide susceptibility and their availability in the study area. We considered factors that are commonly used in landslide susceptibility assessment, such as slope, geology, and land use. We also considered factors that are specific to the study area, such as the distance to the MBT.

Land-use Land Cover:

Land use is a significant factor in landslide susceptibility. Different land uses, such as forest, agricultural land, and barren land, can affect the stability of the land surface. Employing an image classification technique, a land cover map (Figure 5) was generated. The land cover distribution is as follows: forest covers 71.7% of the area, agricultural land occupies 19.1%, barren ground comprises 1.6%, bushes account for 1.4%, water bodies constitute 2.7%, and roads make up 0.6%.

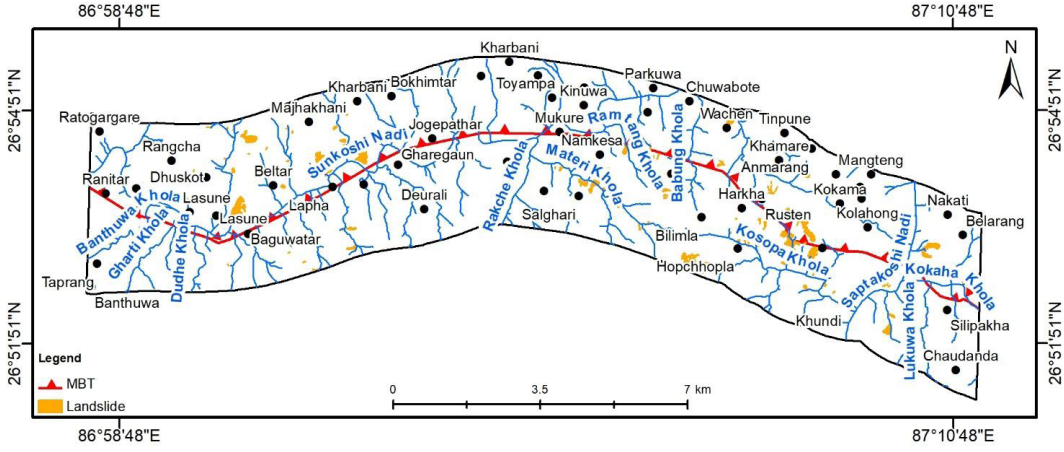

Figure 3. Landslide inventory map (*training & testing datasets)*

Figure 4. Illustration of landslides from study area

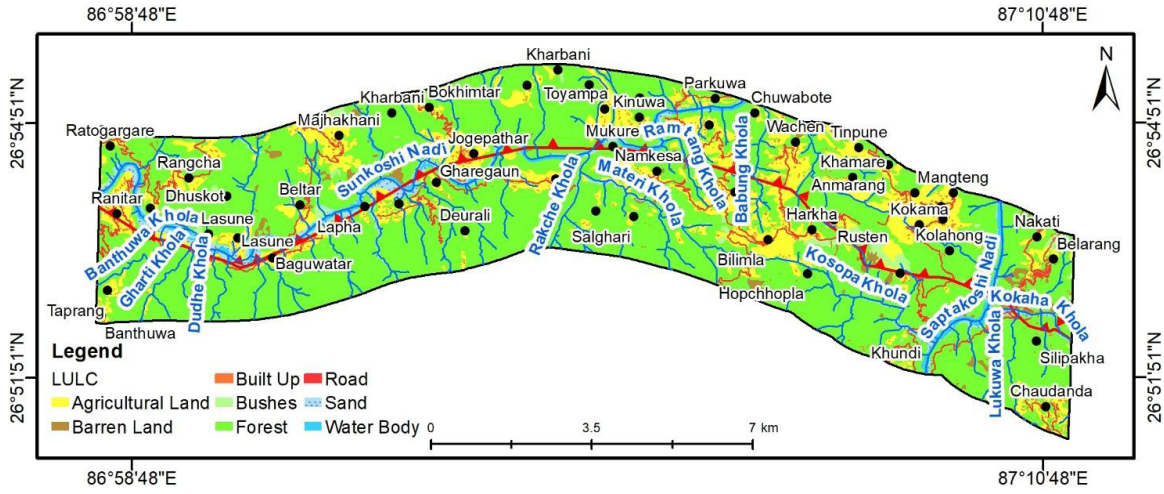

Figure 5. Land-use map of the study area

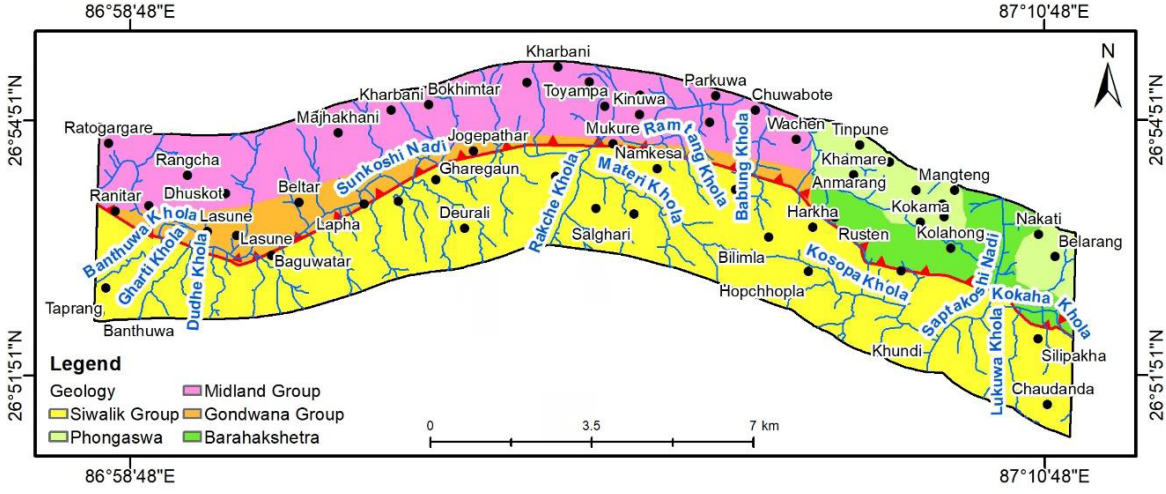

Figure 6. Geological map of the study area

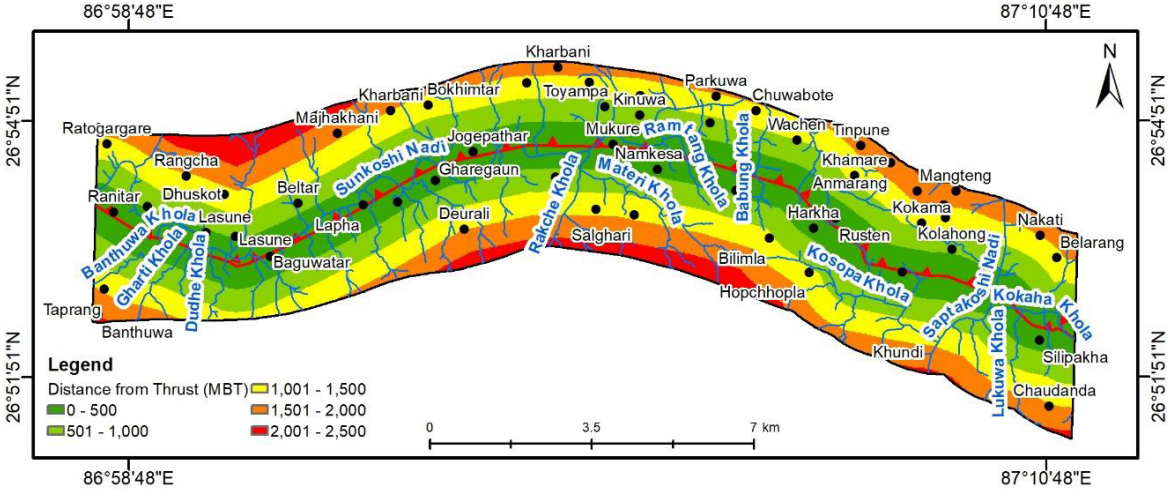

Figure 7. Distance from the Thrust (MBT) map of the study area

Built-up land represents only 0.2% of the total land area. When juxtaposed with the current landslide data, it is observed that barren ground contributes to 52.1% of total landslides, followed by forest at 30.8%, bushes at 10.5%, agricultural land at 3.7%, and roads at 0.04% (refer to Table 2).

Geology:

The geological map obtained from the Department of Mines and Geology (Figure 6) was employed to categorize the study area into five major geological groups: Phongaswa, Barahakshetra, Siwalik Group, Gondwana Group, and Midland Group. According to Table 2, the Siwalik Group predominates the study area, encompassing 50.3% of the total area, while accounting for 49.0% of the total landslides within the same geological context.

Distance to Thrust (MBT):

The distance to the Main Boundary Thrust (MBT) is an important factor in landslide susceptibility. The MBT is a geological fault that can influence the stability of the land surface. The study incorporates the extrinsic parameter known as Distance to Thrust (MBT). Information regarding MBT from petroleum block no. 9 was acquired from the Department of Mines and Geology, Government of Nepal. Subsequently, the block underwent georeferencing, and the MBT locations were delineated from the map. Utilizing both the MBT and the Euclidean distance tools, a Distance to Thrust map (Figure 7) was generated, illustrating the relationship of each cell to a specific source or a combination of sources based on straight-line distance. The map was then segmented into five divisions at 500 m intervals. The investigation revealed that the most vulnerable zone to landslides is within the nearest distance range, i.e., 0 - 500 m. This zone accounted for the highest percentage of landslides, with 40.3% of all occurrences concentrated in this range (Table 2).

Slope:

The slope of the land surface is a critical factor in landslide susceptibility. Steeper slopes are more prone to landslides due to gravity. The Slope map (Figure 8) was generated using a 20*20 Digital Elevation Model (DEM) through the application of the slope algorithm in the Surface-Spatial Analyst Tool within ArcMap. The slope is categorized into seven classes using the equal interval classification method. In Table 2, it is observed that the slope angle ranging from 0° to 20° occupies 12.97% of the total study area, containing 2.2% of total landslides. Similarly, slope angles of 10° to 20°, 20° to 30°, 30° to 40°, 40° to 50°, 50° to 60°, and 60° to 75° cover 15.23%, 28.54%, 29.91%, 11.82%, 1.4%, and 0.14% of the total study area, respectively. Landslides in these respective slope categories are recorded at 4.9%, 22.3%, 39.1%, 26.4%, 5.1%, and 0.1%.

Aspect Map:

The aspect can influence the direction of slope failure. The aspect map (Figure 9) was generated by employing a 20*20 Digital Elevation Model (DEM) through the aspect algorithm in the Surface-Spatial Analyst Tool within ArcMap. The aspect was classified into eight classes, as detailed in Table 2. Analysis indicates that the study area is predominantly characterized by a north-east facing slope, covering 14.2% of the total study area. The second and third most dominant aspects are north (13.2%) and north-west (12.8%) facing slopes, respectively.

Relief Map:

The relief map (Figure 10) for the study area was created utilizing a 20*20 m Digital Elevation Model (DEM). The elevation range spans from a minimum of 120 m to a maximum of 1000 m. The relief map has been categorized into five classes, as outlined in Table 2.

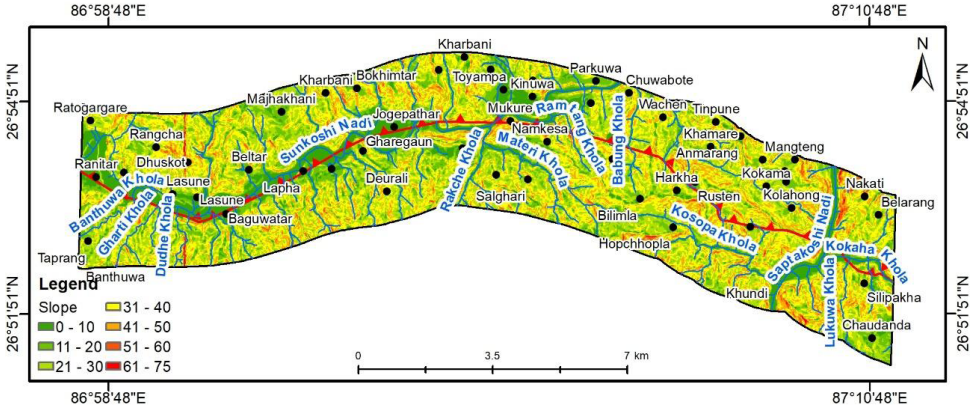

Figure 8. Slope map of the study area

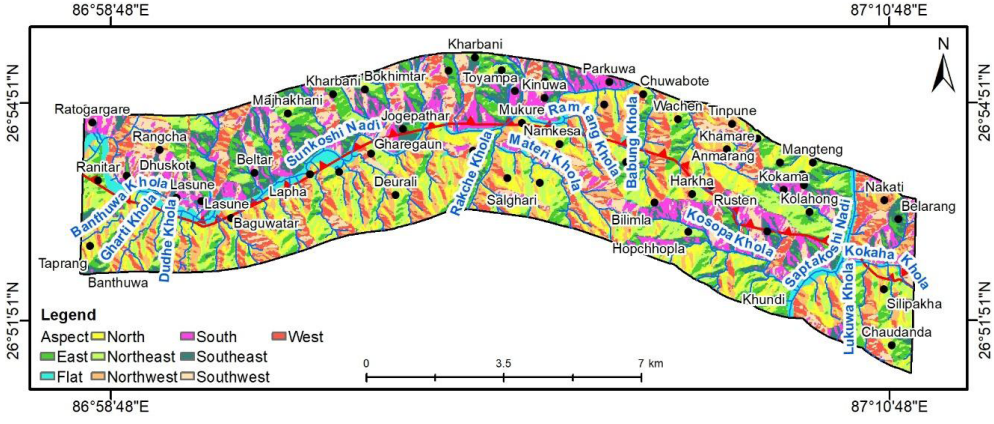

Figure 9. Aspect map of the study area

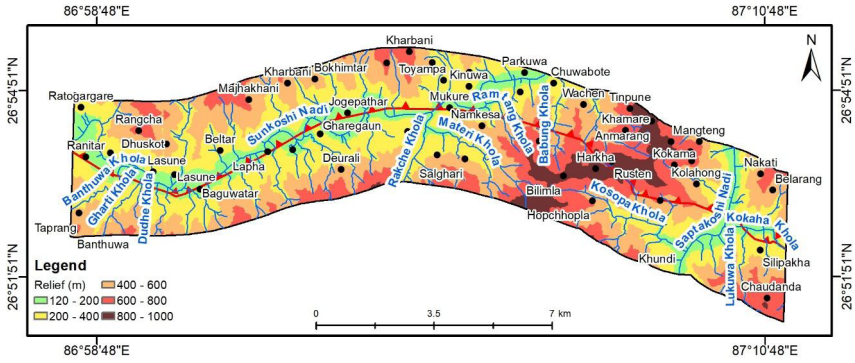

Figure 10. Relief map of the study area (Ranitar - Belarang)

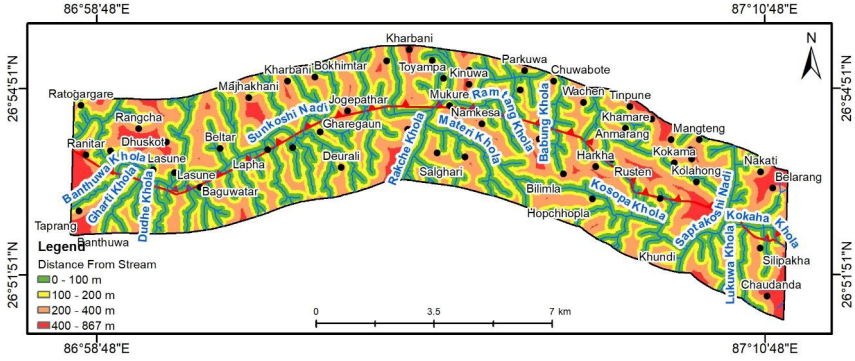

Figure 11. Distance to stream map of the study area

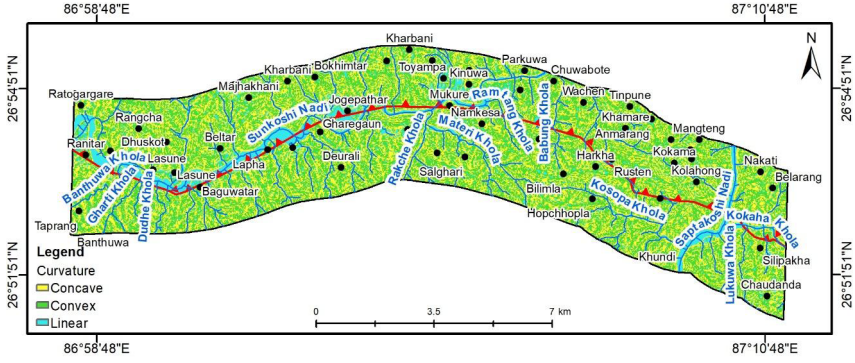

Figure 12. Curvature map of the study area

Distance from Stream:

One of the pivotal factors in landslide susceptibility mapping is the proximity to streams, as areas near streams are more susceptible to landslides due to erosive nature of flowing water.

To assess this, the Distance to Stream map (Figure 11) was created using the Euclidean distance tool, which utilizes straight-line distance to denote each cell's relationship to a source or a collection of sources. The map is categorized into four interval classes. As detailed in Table 2, the region within the 0 to 100 m range from the streams constitutes 38.3% of the total study area and encompasses 38.6% of the total landslides.

Curvature:

Curvature refers to the shape of the Earth's surface. It is a measure of how much a surface deviates from being flat. Curvature can be classified into three types: concave, linear, and convex. Concave surfaces are curved inward, linear surfaces are flat, and convex surfaces are curved outward. In our study, curvature was calculated using a 20*20 m Digital Elevation Model (DEM) and classified into these three categories through the aspect algorithm of the Surface-Spatial Analyst Tool in ArcMap. Curvature is classified into concave, linear, and convex surfaces, as illustrated in Figure 12.

As per Table 2, the study area predominantly exhibits a convex topography, covering 44.4% of the total area, while concave topography accounts for 42.9%. The remaining 12.6% is characterized as a linear or plane surface. Interestingly, a significant portion of landslides, specifically 51.5% of the total, has occurred in concave surfaces.

Distance from Road:

Roads play a crucial role in landslide susceptibility mapping, as areas in proximity to roads are more susceptible to landslides. To assess this, the distance to road map (Figure 13) was generated using the Euclidean distance tool, which characterizes each cell's relationship to a source or set of sources based on straight-line distance. The map is classified into five interval classes (Table 2).

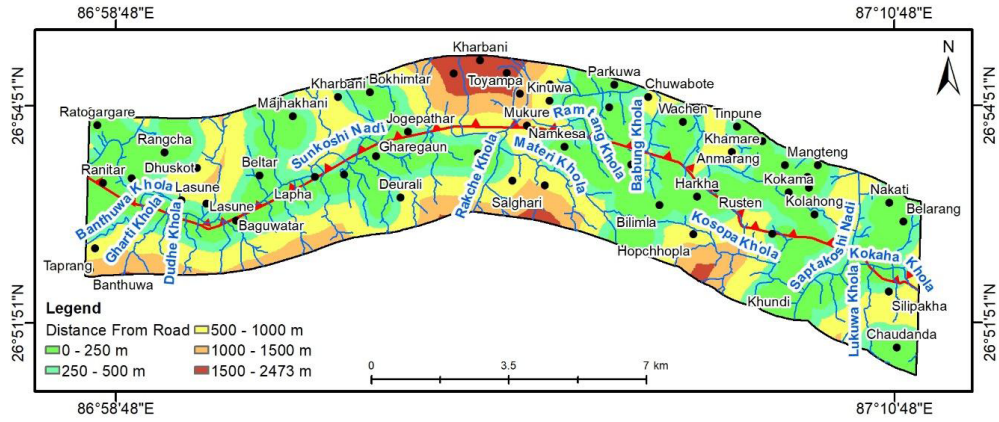

Figure 13. Distance from road map of the study area

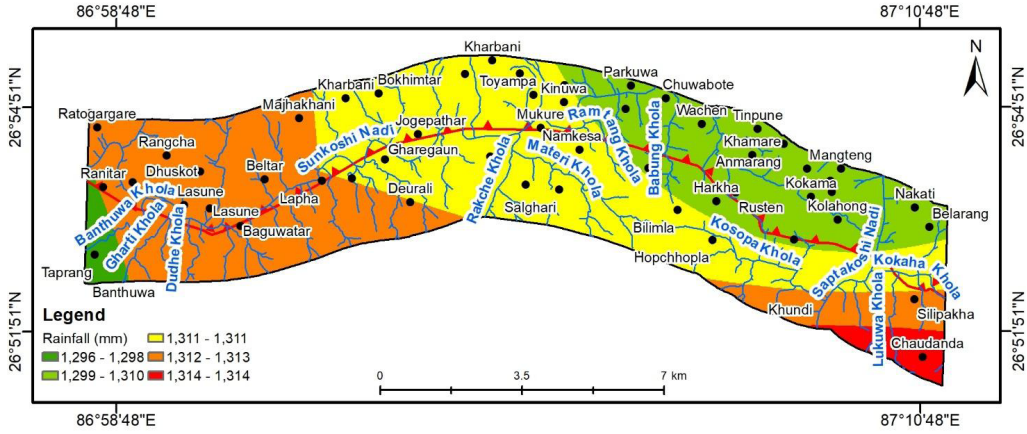

Figure 14. Rainfall map of the study area

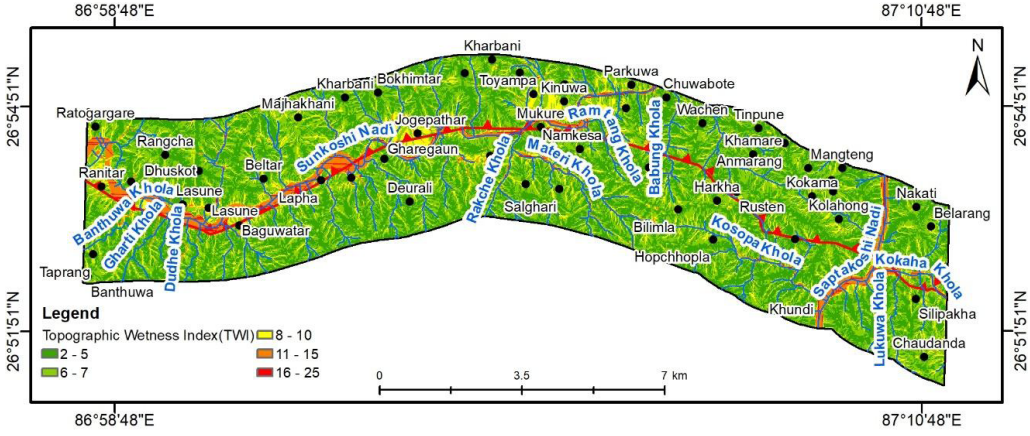

Figure 15. Topographic wetness index map of the study area

Rainfall:

Rainfall infiltration plays an important role in landslide which triggers the sliding of rock mass. On the basis of rainfall data collected from Department of Hydrology and Meteorology, a rainfall map was prepared using IDW method in ArcGIS (Figure 14). In the present study rainfall map was categorized into five classes (Table 2).

Topographic Wetness Index (TWI):

The topography controls the spatial variation of hydrological conditions, like soil moisture, groundwater flow, and slope stability (Yilmaz 2009). The TWI developed by Beven and Kirkby (1979) has been employed for the study.

$$TWI = \ln(A/\tan\beta) \quad 9)$$

where "A" is the specific catchment area and "β" is the local slope angle.

A TWI map (Figure 15) was generated using the flow accumulation derived from Digital Elevation Model (DEM).

Stream Power Index (SPI):

The energy exerted by a river or stream on its surrounding terrain is known as stream power. This force is generated by the interaction of several key factors, including the water's density, its acceleration due to gravity, the volume of water flowing through the channel, and the slope of the water's flow. When these elements combine, they produce a powerful force that can shape the

river's course and surrounding landscape. The SPI measures the erosive power of concentrated surface runoff (Wilson and Gallant, 2000).

The SPI is calculated from the formula: SPI=A* tanβ 10)

where "A" is the specific catchment area and "β" is the local slope angle in degrees.

A SPI map (Figure 16) was generated using the flow accumulation and slope derived from DEM.

Sediment Transport Index (STI):

The STI determines the erosive power of overland flow. STI is denoted mathematically from Moore and Burch (1986) as:

$$STI = \left(\frac{As}{22.13}\right)^{0.16} * \left(\frac{sin\beta}{0.0896}\right)^{1.3} \quad 11)$$

A STI map (Figure 17) was generated using the flow accumulation and slope derived from DEM.

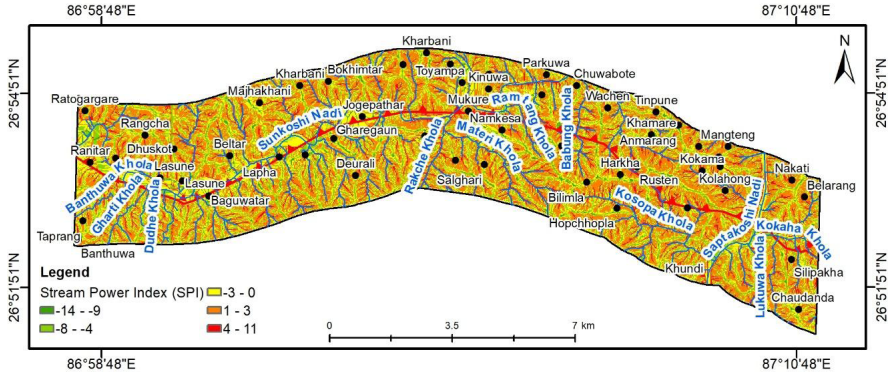

Figure 16. Stream power index map of the study area

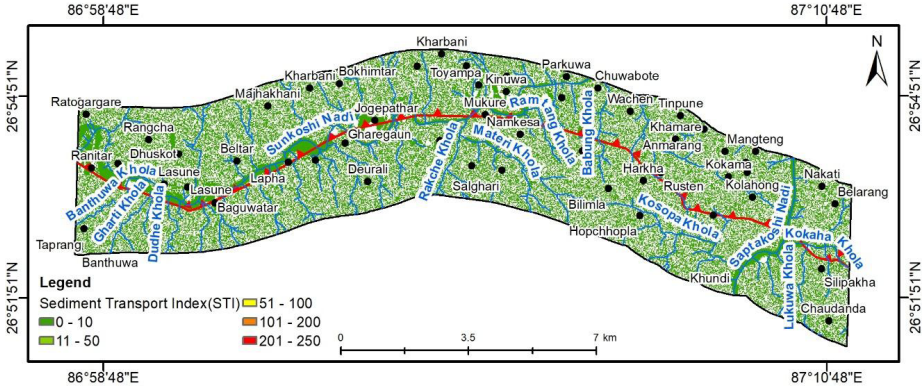

Figure 17. Sediment transport index map of the study area

Table 2. Tabulation of domain with landslide inventory showing area coverage

Domain	Class	Class Pixel	% class pixel	Area (sq. km)	Landslide pixel	% landslide pixel	Area (sq. km)
Slope	**0 - 10**	29089	12.97	11.64	54	2.16	0.02
	10 - 20	34160	15.23	13.66	122	4.87	0.05
	20 - 30	64008	28.54	25.60	559	22.32	0.22
	30 - 40	67100	29.91	26.84	980	39.12	0.39
	40 - 50	26513	11.82	10.61	661	26.39	0.26
	50 - 60	3135	1.40	1.25	127	5.07	0.05
	60 - 75	303	0.14	0.12	2	0.08	0.00
Total		224308	100.00	89.72	2505	100.00	1.00

(*Continued*)

Domain	Class	Class Pixel	% class pixel	Area (sq. km)	Landslide pixel	% landslide pixel	Area (sq. km)
Distance to Thrust (MBT)	**0 - 500 m**	59678	26.59	23.87	1008	40.26	0.40
	500 - 1,000 m	58205	25.94	23.28	761	30.39	0.30
	1,000 - 1,500 m	56506	25.18	22.60	357	14.26	0.14
	1,500 - 2,000 m	39707	17.69	15.88	233	9.31	0.09
	2,000 - 2,630 m	10306	4.59	4.12	145	5.79	0.06
Total		224402	100.00	89.76	2504	100.00	1.00
Landuse	**Agricultural Land**	42718	19.09	17.09	93	3.72	0.04
	Bushes	3148	1.41	1.26	263	10.52	0.11
	Forest	160390	71.69	64.16	770	30.80	0.31
	Sand	6220	2.78	2.49	49	1.96	0.02
	Barren Land	3567	1.59	1.43	1303	52.12	0.52
	Water Body	5958	2.66	2.38	21	0.84	0.01
	Built Up	429	0.19	0.17	0	0.00	0.00
	Road	1285	0.57	0.51	1	0.04	0.00
Total		223715	100.00	89.49	2500	100.00	1.00
Geology	**Phongaswa**	15241	6.79	6.10	94	3.75	0.04
	Barahakshetra	17187	7.66	6.87	348	13.90	0.14
	Siwalik Group	112891	50.31	45.16	1226	48.96	0.49
	Gondwana Group	19607	8.74	7.84	468	18.69	0.19
	Midland Group	59475	26.50	23.79	368	14.70	0.15
Total		224401	100.00	89.76	2504	100.00	1.00
Distance to Stream	**0 - 100 m**	85642	38.25	34.26	965	38.60	0.39
	100 - 200 m	61539	27.49	24.62	671	26.84	0.27
	200 - 400 m	64073	28.62	25.63	808	32.32	0.32
	400 - 867 m	12622	5.64	5.05	56	2.24	0.02
Total		223876	100.00	89.55	2500	100.00	1.00
Curvature	**Concave**	96321	42.94	38.53	1290	51.50	0.52
	Linear	28363	12.64	11.35	112	4.47	0.04
	Convex	99623	44.41	39.85	1103	44.03	0.44
Total		224307	100.00	89.72	2505	100.00	1.00
Aspect	**Flat**	11031	4.92	4.41	13	0.52	0.01
	North	29526	13.16	11.81	209	8.34	0.08
	Northeast	31925	14.23	12.77	236	9.42	0.09
	East	25651	11.44	10.26	214	8.54	0.09
	Southeast	23051	10.28	9.22	445	17.76	0.18
	South	24683	11.00	9.87	472	18.84	0.19
	Southwest	25275	11.27	10.11	596	23.79	0.24
	West	24415	10.88	9.77	182	7.27	0.07
	Northwest	28751	12.82	11.50	138	5.51	0.06
Total		224308	100.00	89.72	2505	100.00	1.00

(*Continued*)

Domain	Class	Class Pixel	% class pixel	Area (sq. km)	Landslide pixel	% landslide pixel	Area (sq. km)
Relief	**120 - 200**	32761	14.61	13.10	120	4.79	0.05
	200 - 400	77207	34.42	30.88	1046	41.76	0.42
	400 - 600	68392	30.49	27.36	771	30.78	0.31
	600 - 800	36149	16.12	14.46	392	15.65	0.16
	800 - 1000	9799	4.37	3.92	176	7.03	0.07
Total		224308	100.00	89.72	2505	100.00	1.00
Distance to Road	**0 - 250 m**	83091	37.11	33.24	528	21.12	0.21
	250 - 500 m	51170	22.86	20.47	647	25.88	0.26
	500 - 1000 m	62178	27.77	24.87	1157	46.28	0.46
	1000 - 1500 m	21282	9.51	8.51	168	6.72	0.07
	1500 - 2473 m	6155	2.75	2.46	0	0.00	0.00
Total		223876	100.00	89.55	2500	100.00	1.00
Stream Power Index (SPI)	**(-14 - -9)**	3372	1.5	11	0.4	0.29	0.06
	(-8 - -4)	44144	19.9	405	16.2	0.81	0.18
	(-3 - 0)	64957	29.3	480	19.2	0.66	0.14
	(1 - 3)	90865	41.0	1280	51.2	1.25	0.27
	(4 - 11)	18392	8.3	323	12.9	1.56	0.34
Total		221730	100.0	2499	100.0	4.57	1.00
Sediment Transport Index (STI)	**0 - 10**	116296	99.1	1240	99.2	1.00	0.49
	11 -- 50	887	0.76	10	0.80	1.06	0.51
	51 - 100	74	0.1	0.0	0.0	0.00	0.00
	101 - 200	86	0.1	0.0	0.0	0.00	0.00
	201 - 250	8	0.0	0.0	0.0	0.00	0.00
Total		117351	100.0	1250.0	100.0	2.06	1.00
Topographic Wetness Index (TWI)	**(2 - 5)**	98047	43.7	1233	49.3	1.13	0.31
	(6 - 7)	82965	37.0	932	37.2	1.01	0.28
	(8 - 10)	26738	11.9	259	10.3	0.87	0.24
	(11 - 15)	14008	6.2	74	3.0	0.47	0.13
	(16 - 25)	2536	1.1	5	0.2	0.18	0.05
Total		224294	100.0	2503	100.0	3.65	1.00
Rainfall	**1,296 - 1,298**	3197	1.4	0	0.0	0.00	0.00
	1,299 - 1,310	30970	13.8	264	10.5	0.76	0.20
	1,311 - 1,311	65071	29.0	1144	45.7	1.58	0.41
	1,312 - 1,313	73372	32.7	809	32.3	0.99	0.26
	1,314 - 1,314	51792	23.1	287	11.5	0.50	0.13
Total		224402	100.0	2504	100.0	3.82	1.00

Table 3. Weightage of each class of thirteen contributing factors based on WoE, AHP, and FR.

Domain	Class	% class pixel	% landslide pixel	Weight of Evidence (WoE)	Analytical Hierarchy Process (AHP) Weightage	Frequency Ratio (FR)	Relative Frequency (RF)	RF (Non %)	PR
Slope	**0 - 10**	12.97	2.2	-1.804	0.03	0.17	0.02	1.84	1.96
	10 - 20	15.23	4.9	-1.148	0.044	0.32	0.04	3.54	
	20 - 30	28.54	22.3	-0.248	0.067	0.78	0.09	8.66	
	30 - 40	29.91	39.1	0.272	0.104	1.31	0.14	14.49	
	40 - 50	11.82	26.4	0.817	0.159	2.23	0.25	24.73	
	50 - 60	1.40	5.1	1.319	0.241	3.63	0.40	40.19	
	60 - 75	0.14	0.1	-0.530	0.351	0.59	0.07	6.55	
Total		**100.0**	**100.0**	**-**	**1.00**	**9.03**	**1.00**	**100.00**	
Distance to Thrust (MBT)	**0 - 500 m**	26.6	40.3	0.420	0.417	1.51	0.30	30.04	1.00
	500 - 1,000 m	25.9	30.4	0.160	0.263	1.17	0.23	23.26	
	1,000 - 1,500 m	25.2	14.3	-0.574	0.16	0.57	0.11	11.24	
	1,500 - 2,000 m	17.7	9.3	-0.648	0.097	0.53	0.10	10.44	
	2,000 - 2,630 m	4.6	5.79	0.235	0.061	1.261	0.250	25.03	
Total		100.0	100.0	-	1.00	5.04	1.00	100.00	
Landuse	**Agricultural Land**	19.1	3.7	-1.645	0.105	0.19	0.00	0.47	3.98
	Bushes	1.4	10.5	2.088	0.231	7.48	0.18	17.85	
	Forest	71.7	30.8	-0.851	0.046	0.43	0.01	1.03	
	Sand	2.8	2.0	-0.353	0.03	0.70	0.02	1.68	
	Barren Land	1.6	52.1	3.930	0.328	32.69	0.78	78.05	
	Water Body	2.7	0.8	-1.162	0.034	0.32	0.01	0.75	
	Built Up	0.2	0.00	0.000	0.069	0.00	0.00	0.00	
	Road	0.6	0.04	-2.675	0.157	0.07	0.00	0.17	
Total		**100.0**	**100.0**	**-**	**1**	**41.88**	**1.00**	**100.00**	
Geology	**Phongaswa**	6.8	3.8	-0.598	0.061	0.55	0.09	9.16	1.34
	Barahakshetra	7.7	13.9	0.605	0.097	1.81	0.30	30.07	
	Siwalik Group	50.3	49.0	-0.027	0.417	0.97	0.16	16.13	
	Gondwana Group	8.7	18.7	0.773	0.16	2.14	0.35	35.45	
	Midland Group	26.5	14.7	-0.595	0.263	0.55	0.09	9.19	
Total		**100.0**	**100.0**	**-**	**1.00**	**6.03**	**1.00**	**100.00**	
Distance to Stream	**0 - 100 m**	38.3	38.6	0.009	0.466	1.01	0.29	28.73	1.06
	100 - 200 m	27.5	26.8	-0.024	0.277	0.98	0.28	27.80	
	200 - 400 m	28.6	32.3	0.123	0.16	1.13	0.32	32.15	
	400 - 867 m	5.6	2.2	-0.930	0.095	0.40	0.11	11.31	
Total		**100.0**	**100.0**	**-**	**1.00**	**3.51**	**1.00**	**100.00**	
Curvature	**Concave**	42.9	51.5	0.184	0.539	1.20	0.47	47.14	1.70
	Linear	12.6	4.5	-1.047	0.163	0.35	0.14	13.90	
	Convex	44.4	44.0	-0.009	0.296	0.99	0.39	38.97	
Total		**100.0**	**100.0**	**-**	**1.00**	**2.54**	**1.00**	**100.00**	

(*Continued*)

Domain	Class	% class pixel	% landslide pixel	Weight of Evidence (WoE)	Analytical Hierarchy Process (AHP) Weightage	Frequency Ratio (FR)	Relative Frequency (RF)	RF (Non %)	PR
Aspect	Flat	4.9	0.52	-2.259	0.016	0.1	0.01	1.20	1.16
	North	13.2	8.34	-0.460	0.108	0.6	0.07	7.20	
	Northeast	14.2	9.42	-0.416	0.072	0.66	0.08	7.52	
	East	11.4	8.54	-0.294	0.03	0.75	0.08	8.49	
	Southeast	10.3	17.76	0.556	0.158	1.73	0.20	19.65	
	South	11.0	18.84	0.546	0.316	1.71	0.19	19.46	
	Southwest	11.3	23.79	0.760	0.227	2.11	0.24	24.00	
	West	10.9	7.27	-0.408	0.02	0.7	0.08	7.59	
	Northwest	12.8	5.51	-0.851	0.048	0.4	0.05	4.89	
Total		**100.0**	**100.00**	**-**	**1.00**	**9**	**1**	**100**	
Relief	120 - 200	14.6	4.8	-1.122	0.061	0.33	0.06	6.39	1.27
	200 - 400	34.4	41.8	0.196	0.097	1.21	0.24	23.65	
	400 - 600	30.5	30.8	0.010	0.16	1.01	0.20	19.68	
	600 - 800	16.1	15.6	-0.030	0.263	0.97	0.19	18.93	
	800 - 1000	4.4	7.0	0.482	0.417	1.61	0.31	31.35	
Total		**100.0**	**100.0**	**-**	**1.00**	**5.13**	**1**	**100**	
DisRoad	0 - 250 m	37.1	21.1	-0.569	0.417	0.57	0.14	13.97	2.09
	250 - 500 m	22.9	25.9	0.126	0.263	1.13	0.28	27.79	
	500 - 1000 m	27.8	46.3	0.518	0.16	1.67	0.41	40.90	
	1000 - 1500 m	9.5	6.7	-0.350	0.097	0.71	0.17	17.35	
	1500 - 2473 m	2.7	0.0	0.000	0.061	0.00	0.00	0.00	
Total		**100.0**	**100**	**-**	**1.00**	**4.07**	**1.00**	**100**	
SPI	(-14 - -9)	1.5	0.4	-1.248	0.061	0.29	0.06	6.34	1.42
	(-8 - -4)	19.9	16.2	-0.208	0.097	0.81	0.18	17.82	
	(-3 - 0)	29.3	19.2	-0.426	0.16	0.66	0.14	14.36	
	(1 - 3)	41.0	51.2	0.226	0.263	1.25	0.27	27.37	
	(4 - 11)	8.3	12.9	0.450	0.417	1.56	0.34	34.12	
Total		**100.0**	**100.0**	**-**	**1.00**	**4.57**	**1.00**	**100.00**	
STI	0 - 10	99.1	99.2	0.001	0.061	1.00	0.49	48.61	2.62
	11 -- 50	0.76	0.80	0.057	0.097	1.06	0.51	51.39	
	51 - 100	0.1	0.0	0.000	0.16	0.00	0.00	0.00	
	101 - 200	0.1	0.0	0.000	0.263	0.00	0.00	0.00	
	201 - 250	0.0	0.0	0.000	0.417	0.00	0.00	0.00	
Total		**100.0**	**100.0**	**-**	**1.00**	**2.06**	**1.00**	**100.00**	
TWI	(2 - 5)	43.7	49.3	0.121	0.065	1.13	0.31	30.86	1.33
	(6 - 7)	37.0	37.2	0.007	0.099	1.01	0.28	27.57	
	(8 - 10)	11.9	10.3	-0.143	0.162	0.87	0.24	23.77	
	(11 - 15)	6.2	3.0	-0.754	0.267	0.47	0.13	12.96	
	(16 - 25)	1.1	0.2	-1.743	0.405	0.18	0.05	4.84	
Total		**100.0**	**100.0**	**-**	**1.00**	**3.65**	**1.00**	**100.00**	

(*Continued*)

Domain	Class	% class pixel	% landslide pixel	Weight of Evidence (WoE)	Analytical Hierarchy Process (AHP) Weightage	Frequency Ratio (FR)	Relative Frequency (RF)	RF (Non %)	PR
Rainfall	**1,296 - 1,298**	1.4	0.0	0.000	0.061	0.00	0.00	0.00	2.10
	1,299 - 1,310	13.8	10.5	-0.272	0.097	0.76	0.20	19.98	
	1,311 - 1,311	29.0	45.7	0.461	0.16	1.58	0.41	41.20	
	1,312 - 1,313	32.7	32.3	-0.012	0.263	0.99	0.26	25.84	
	1,314 - 1,314	23.1	11.5	-0.706	0.417	0.50	0.13	12.99	
Total		**100.0**	**100.0**	**-**	**1.00**	**3.82**	**1.00**	**100.00**	

4. Results

Landslide susceptibility based on Frequency Ratio Method (FR):

In Ranitar - Belarang section, 20% of the total area fall in an unstable zone as shown in the final susceptibility map (Figure 19), generated using thirteen influencing factor maps. The high susceptibility zone encompasses Silipakha, Khecha, Kinuwa, Beltar, Lasune, Byangtar, Taprang, and Ranitar. Conversely, the remaining communities fall into either a low or extremely low vulnerable zone. Of the total study area, 60% is categorized as stable (Banthuwa, Rangcha, Rato Gharghare, Baguwatar, Lapha, Ghurguredanda, Gharegaun, Majhakhani, Kharbani, Bokhimtar, Jogepathar, Magarmukha, Baksikhop, Pipalbote, Toyampa, Hangdang, Salghari, Namkesa, Khawatang, Mukure, Parkuwa, Mainatar, Dankha, Chuwabote, Wachen, Bilimla, Harkha, Khamare, Tinpune, Anmarang, Hangmachong, Kokama, Mulgaun, Mangteng, Kolahong, Khundi, Belarang, Barahaksetra, and Chaudanda), while 20% is quasi stable, and 20% of the study area is unstable. This distribution is further detailed in Figure 21 and Table 6.

Table 4. Weight of individual factor

Domain/Factor	PR
Distance to Thrust	1.00
Distance to stream	1.06
Aspect	1.16
Relief	1.27
TWI	1.33
Geology	1.34
SPI	1.42
Distance to Road	1.66
Curvature	1.70
Slope	1.96
Rainfall	2.10
STI	2.62
Landuse	3.98

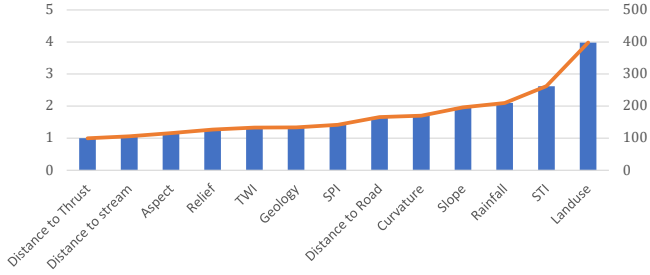

Figure 18. Graph showing weight of individual factor

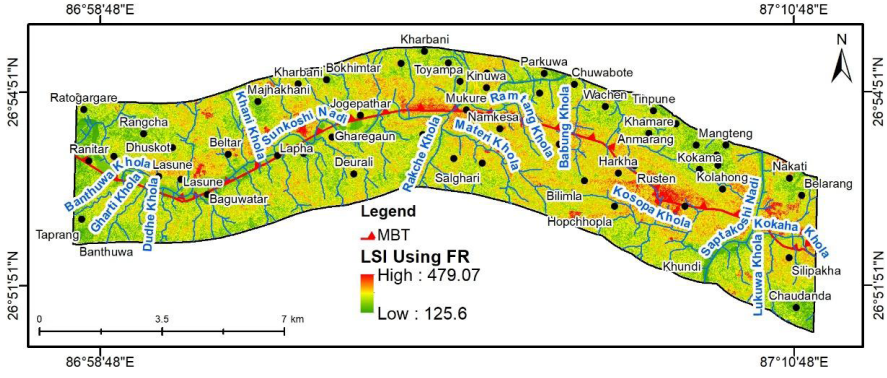

Figure 19. Landslide susceptibility index map of the study area using FR method.

Equation (2) was used to create the Landslide Susceptibility Index (LSI). To categorize the LSI data, we applied the Receiver Operating Characteristic/ Area Under the Curve (ROC/AUC) curve. The LSI, representing the likelihood of landslides, was qualitatively examined using success rate curves in IBM-SPSS Statistics 20. This helped us evaluate how well the proposed frequency approach predicts potential landslide zones.

In Figure 20, the ROC/AUC analysis yielded a measurement of 0.864, signifying a prediction accuracy of 86.4% with an upper limit of 87.2%. This means our prediction is reliable. Regarding landslide potential, the success rate revealed that in 20% of the study area, a high rank is assigned, explaining 78% of all landslides in that region. Similarly, 40% of the suggested Landslide Susceptibility Index (LSI) values can clarify around 88% of all existing landslides.

As a result, three landslide susceptibility classes were established as: Stable (greater than 40%), Quasi Stable (20-40%), and Unstable (0-20%). We classified the LSI into these zones with threshold values for the respective classes set at 279.32, 302.78, and 479.07, as outlined in Table 5. These thresholds were employed to create the final landslide susceptibility map (Figure 21).

Landslide Susceptibility based on Analytical Hierarchy Process (AHP):

The final susceptibility map (Figure 23), generated using thirteen influencing factor maps, designates Ranitar - Belarang section's 25.94% of total area as an unstable zone. The high susceptibility zone encompasses Khundi, Harkha, Baksikhop, Khecha, Beltar, Bilimla, Baguwatar, and Ratogargare. Of the total study area, 28.62% is categorized as stable (Silipakha, Chaudanda, Wachen, Tinpune, Anmarang, Khamare, Hangmachong, Mangteng, Mulgaun, Barigaun, Rusten, Nakati, Kolahong, Belarang, Dhakmalung, Barahaksetra, Kharbani, Pipalbote, Magarmukha, Khawatang, Bokhimtar, Toyampa, Kharbani, Chuwabote, Kinuwa, Mainatar, Majhakhani, Mukure, Dankha, Jogepathar, Namkesa, Gharegaun, Dhuskot, Ghurghuredanda, Lapha, Hangdang, Salghari, Deurali, Lasune, Ranitar, and Banthuwa), while 45.43% of the study area including the settlement area which includes Kokama, Delukha, Hopchhopla, Parkuwa, Rangcha, Byangtar, Lasune, and Taprang is categorized as quasi stable. This distribution is further detailed in Figure 23 and Table 6.

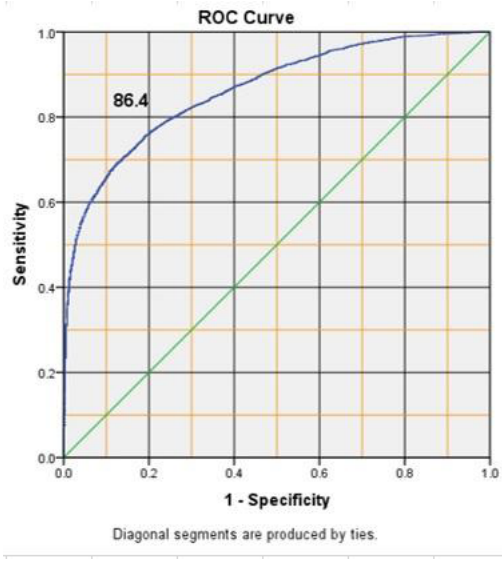

Case Processing Summary				
Slide[a]	Valid N (listwise)			
Positive[b]	2535			
Negative	219174			
Larger values of the test result variable(s) indicate stronger evidence for a positive actual state.				
a. The test result variable(s): LSI has at least one tie between the positive actual state group and the negative actual state group.				
b. The positive actual state is 1.				

Area Under the Curve				
Test Result Variable(s): LSI				
			Asymptotic 95% Confidence Interval	
Area	Std. Error[a]	Asymptotic Sig.[b]	Lower Bound	Upper Bound
.864	.004	0.000	.856	.872
The test result variable(s): LSI has at least one tie between the positive actual state group and the negative actual state group. Statistics may be biased.				
a. Under the nonparametric assumption				
b. Null hypothesis: true area = 0.5				

Figure 20. ROC/AUC Curve of Ranitar - Belarang LSI model using FR method

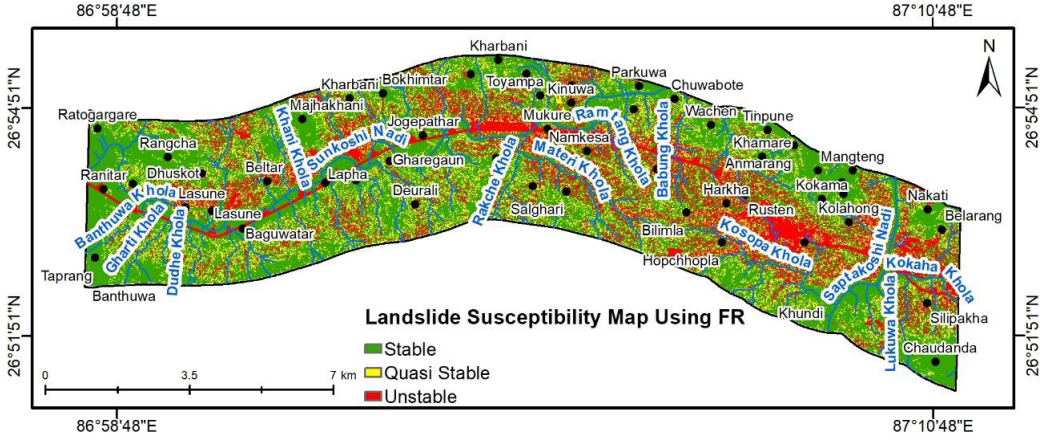

Figure 21. Landslide Susceptibility map of the Study area using FR method

Following the approach of Table 1, Weightage of each class of thirteen parameters was obtained (Table 3) and was employed to construct the Landslide Susceptibility Index (LSI) using AHP method.

In Figure 22, the ROC/AUC analysis showed a measurement of 0.685, indicating a prediction accuracy of 68.5% with an upper limit of 69.5%. This analysis is considered valid. Regarding landslide potential, the success rate revealed that in 20% of the study area, a high rank is assigned, explaining 45% of all landslides in that region. Similarly, 40% of the suggested Landslide Susceptibility Index (LSI) values can clarify around 67.5% of all existing landslides.

Consequently, we established three landslide susceptibility classes: Stable zone (60%), Quasi Stable (80-60%), and Unstable (90-100%). The LSI was classified into these zones with threshold values for the respective classes set at 2.28, 2.72, and 4.16, as outlined in Table 5. These thresholds were used to create the final landslide susceptibility map (Figure 23).

Landslide Susceptibility based on Weight of Evidence (WoE):

The final susceptibility map (Figure 25), generated using thirteen influencing factor maps in Ranitar - Belarang section shows 19.87% of total area as unstable zone. The high susceptibility zone encompasses Nakati. Major regions in between Delukha and Dhakmalung village, and western region of the study area (North of Sunkoshi Nadi). Of the total study area, 60.19% is categorized as stable (Khundi, Chaudanda, Wachen, Tinpune, Anmarang, Khamare, Hangmachong, Mangteng, Mulgaun, Barigaun, Rusten, Kokama, Harkha, Kolahong, Belarang, Dhakmalung, Hopchhopla, Barahaksetra, Kharbani, Pipalbote, Magarmukha, Khawatang, Parkuwa, Bokhimtar, Toyampa, Kharbani, Chuwabote, Mainatar, Majhakhani, Mukure, Dankha, Jogepathar, Namkesa, Baksikhop, Gharegaun, Dhuskot, Ghurghuredanda, Beltar, Lapha, Hangdang, Salghari, Lasune, Bilimla, Baguwatar, Ratogargare, Rangcha, Ranitar, Taprang, and Banthuwa), while 19.87% is quasi stable (settlements: Silipakha, Delukha, Kinuwa, Khecha, Deurali, Byangtar, and Lasune). This distribution is further detailed in Figure 25 and Table 6.

Equation (7 & 8) was utilized to create the Landslide Susceptibility Index (LSI). The Receiver Operating Characteristic/Area Under the Curve (ROC/AUC) curve was employed to categorize the LSI data. Qualitative analysis of the LSI (Landslide Susceptibility Index) was conducted using success rate curves in IBM-SPSS Statistics 20, aiming to evaluate the effectiveness of the proposed frequency approach in identifying potential landslide zones.

In the provided diagram (Figure 24), the area under the success rate curve (ROC/AUC) measures at 0.899, indicating a prediction rate of 89.9% with an upper boundary of 90.6%. This analysis is considered valid. Regarding landslide potential, the success rate reveals that in 20% of the study area, a high rank is assigned, explaining 80% of all landslides in that region. Similarly, 40% of the suggested Landslide Susceptibility Index (LSI) values can clarify around 91% of all existing landslides.

As a result, three landslide susceptibility classes were defined: Stable zone (60%), Quasi Stable (60-80%), and Unstable (80 -100%). The LSI was categorized into these zones with threshold values for the respective classes set at -1.27, -0.26, and 8.6 as detailed in Table 5. These thresholds were used to generate the final landslide susceptibility map (Figure 25).

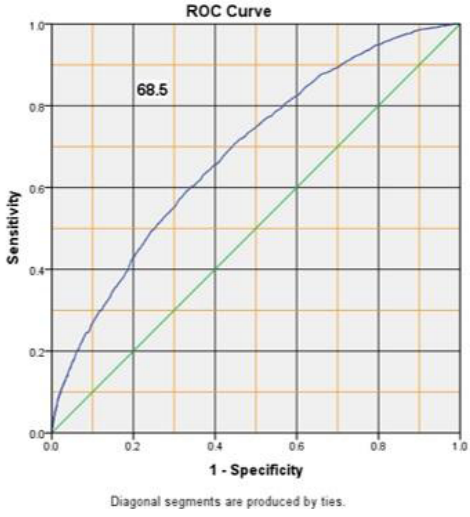

Case Processing Summary				
Landslide[a]	Valid N (listwise)			
Positive[b]	2535			
Negative	219174			
Larger values of the test result variable(s) indicate stronger evidence for a positive actual state.				
a. The test result variable(s): LSI has at least one tie between the positive actual state group and the negative actual state group.				
b. The positive actual state is 1.				
Area Under the Curve				
Test Result Variable(s): LSI				
Area	Std. Error[a]	Asymptotic Sig.[b]	Asymptotic 95% Confidence Interval	
			Lower Bound	Upper Bound
.685	.005	.000	.675	.695
The test result variable(s): LSI has at least one tie between the positive actual state group and the negative actual state group. Statistics may be biased.				
a. Under the nonparametric assumption				
b. Null hypothesis: true area = 0.5				

Figure 22. ROC/AUC Curve of Ranitar - Belarang LSI model using AHP method.

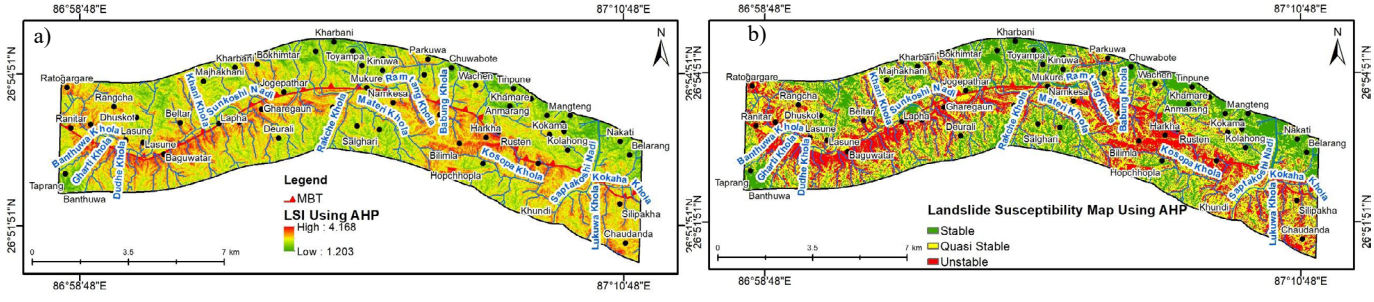

Figure 23. (a) Landslide Susceptibility Index and (b) Landslide Susceptibility Map based on AHP method.

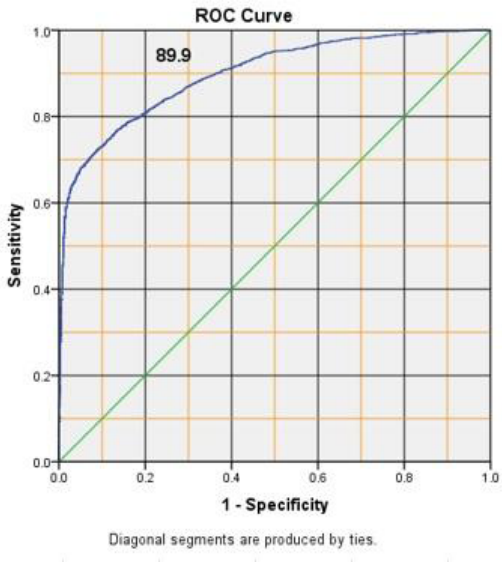

Case Processing Summary	
Slide[a]	Valid N (listwise)
Positive[b]	2535
Negative	219174

Larger values of the test result variable(s) indicate stronger

a. The test result variable(s): LSI has at least one tie between the positive actual state group and the negative actual state group.

b. The positive actual state is 1.

Area Under the Curve

Test Result Variable(s): LSI

Area	Std. Error[a]	Asymptotic Sig.[b]	Asymptotic 95% Confidence Interval	
			Lower Bound	Upper Bound
.899	.004	0.000	.892	.906

The test result variable(s): LSI has at least one tie between the positive actual state group and the negative actual state group. Statistics may be biased.

a. Under the nonparametric assumption

b. Null hypothesis: true area = 0.5

Figure 24. ROC/AUC Curve of Ranitar - Belarang LSI model using WoE method.

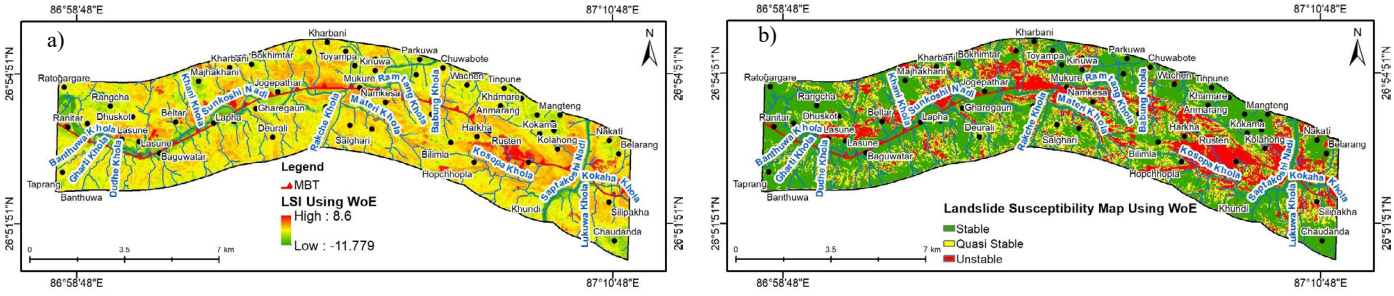

Figure 25. (a) Landslide Susceptibility Index and (b) Landslide Susceptibility Map based on WoE method.

Table 5. Boundary value set for different susceptibility classes

Method of Analysis	Cumulative %	Class Name	LSI
			Upper Bound
Frequency Ratio Method (FR)	60%	Stable Zone	279.32
	80%	Quasi Stable Zone	302.78
	100%	Unstable Zone	479.07
Analytical Hierarchy Process (AHP)	60%	Stable Zone	2.28
	80%	Quasi Stable Zone	2.72
	100%	Unstable Zone	4.16
Weight of Evidence (WoE)	60%	Stable Zone	-1.27
	80%	Quasi Stable Zone	-0.26
	100%	Unstable Zone	8.6

Table 6. Area coverage by different landslide susceptibility class.

Class	Count	Area (sq. km)	Area %	Classification Method
Landslide Susceptibility (Frequency Ratio Method)				
Stable	133018	53.2	60.01%	ROC/AUC Curve
Quasi Stable	44344	17.73	20.00%	
Unstable	44347	17.73	20.00%	
Total	221709	88.66	100.00%	
Landslide Susceptibility (Analytical Hierarchy Process)				
Stable	63470	25.38	28.62%	ROC/AUC Curve
Quasi Stable	100717	40.28	45.43%	
Unstable	57522	23	25.94%	
Total	221709	88.66	100%	
Landslide Susceptibility (Weight of Evidence)				
Stable	133439	53.37	60.19%	ROC/AUC Curve & WoE
Quasi Stable	44072	17.62	19.87%	
Unstable	44198	17.67	19.87%	
Total	221709	88.66	100%	

Discussions:

This study aimed to evaluate accuracy of FR, AHP, and WoE methods for predicting landslide susceptibility in the Ranitar-Belarang area of Udayapur district. Thirteen causative factors; geology, slope, aspect, curvature, distance from the stream, distance from the road, distance from the thrust (MBT), relief, land use land cover, rainfall, topographic wetness index, stream power index and sediment transport index were considered. The selection of contributing factors was based on the presence or absence of factors and their importance. The selection of analysis methods was based on widely accepted literatures ((Bhandari et al., 2024; Demir et al., 2013; Ding et al., 2017; Pokhrel & Bhandari, 2019; Thapa & Bhandari, 2019) and their effectiveness on predicting landslide susceptibility. Both the Frequency Ratio (FR) and Weight of Evidence (WoE) models have their merits in landslide susceptibility mapping. The FR model is known for its simplicity and ease of interpretation, making it a popular choice among researchers. On the other hand, the WoE model has demonstrated superior accuracy and user-friendliness in predicting landslide likelihood. AHP helps decision makers to prioritize factors and assign weights based on their relative importance in landslide susceptibility assessment. It provides a structured approach to combine subjective judgments and objective data ((Demir et al., 2013).

The utilization of Digital Elevation Model (DEM) proves to be crucial in landslide studies, as evidenced by research (Kamp et al., 2008; Wang et al., 2015). Although there is no direct relationship between elevation and landslide occurrence, studies suggest an increased probability of landslide events at higher elevations (Ercanoglu et al., 2004). The concentration of landslides was found to be maximum in the elevation range of 500 m-750 m.

The steepness of the slope is another significant topographic factor considered in landslide susceptibility studies (Kamp et al., 2008; Pradhan & Lee, 2010; Regmi et al., 2016; Regmi et al., 2010; Wang et al., 2015). Among the slope, ranging from 0°-75°, it was revealed maximum landslide concentration in the slope range of 30°-50°.

The aspect of the slope, influencing moisture retention and its relation to the attitude of bedding of the rock formation, plays a role in affecting the physical properties of slope material and its susceptibility to failure (Dai et al., 2001). In this study, aspects to the south, southwest, and southeast contribute significantly to landslides. This is often attributed to the fact that many rivers' segments trend towards SW-SE, and landslides appear on slopes facing the river.

The surface undulation of the slope is identified as a major factor triggering landslides, as it strongly influences slope instability. In the case of curvatures, landslides are typically distributed in convex and concave slopes. Convex slopes, in particular, are noted for earthquake-induced landslides (Reneau & Dietrich, 1987). In the study area, concave slopes dominate over convex slopes by 1.5%.

Land-use is recognized as a significant landslide conditioning factor due to its potential to influence vegetation cover, thereby affecting mechanical factors such as soil strength and slope behavior, as well as hydrological aspects (Greenway, 1987; Reichenbach et al., 2014; van Westen et al., 2003). The variation in land-use distribution can be attributed to natural processes, human activities, or a combination of both. In this study, the land-use map was generated through manual digitization of a satellite image (Google Earth Image) of the study area. It was found that the landslide occurred mostly on the barren land.

The derived weights, obtained through the Frequency Ratio Method, Analytical Hierarchy Process, and Weight of Evidence highlight the significant impact of terrain slope on landslide distribution. Generally, landslide occurrences increase with an increase in terrain gradient. This observation is reinforced by the analysis, where the slope gradient of 50^{o} – 60^{o} has the highest frequency ratio (FR) value of 3.63, WoE of 1.319 and AHP of 0.241 making it the most prone to landslides. In contrast, terrain with a slope gradient of $<10^{o}$ is least prone to landslides, with a frequency ratio of 0.17 (Table 3).

The vicinity in the range of 0 to 250 m distance from the road covers most of the study area (37.11 % of the study area) and covers 21.1% of total landslide. However, most of the landslide (46.3%) falls under the area ranging distance of 500 - 1000 m from the road. The associated values for WoE, AHP and FR for 500-1000 class are 0.518, 0.16, and 1.67 respectively.

While the area within 0-100 m from the streams has a frequency ratio of 1.01, WoE of 0.009 and AHP of 0.466, the highest FR and WoE value is observed at the distance of 200 – 400 m. This discrepancy may be attributed to other parameters such as thrust, land-use, slope, and curvature playing a more influential role in triggering landslides.

Regarding land use land cover, barren land has the highest frequency ratio of 32.69, WoE of 3.93, and AHP of 0.328 followed by bushes with an FR of 7.48, WoE of 2.088, and AHP of 0.231. The FR, WoE, and AHP weight values assigned to barren land and bush land, are identified as stronger than those for other land-use classes. This underscores the significance of barren land and bush land in contributing to landslide susceptibility. The analysis in Table 3 indicates

that concave curvature has a high frequency of landslide occurrence, with a value of 1.20, WoE of 0.184, and AHP of 0.539. Additionally, it was observed that most landslides occur in the Siwalik zone, with a frequency ratio of 0.97, with WoE of -0.027 which represents negative relationship with the landslide, and AHP of 0.417 (Neupane and Paudyal, 2021). However, the Gondwana Group has the highest frequency ratio of 2.14 among all other geology present in the area, WoE of 0.773, and AHP of 0.16. This is because the Gondwana Group, covering 8.7% of the total area, has landslides covering 18.7% of the total landslide area in the study area. The zone closest to the thrust (MBT) has the largest number of landslides, with a frequency ratio of 1.51, WoE of 0.42, and AHP of 0.147 indicating that the 0-500 m distance is the most prone to landslides. The similar type of results was obtained in the previous studies in the Nepal Himalaya in different sections (Paudyal and Maharjan, 2022 & 2023; Neupane et al, 2023; Shahi et al, 2022). As a prime cause of landslide, in Nepal Himalaya, is found the presence of adverse geological structures like the active faults and thrust (Acharya and Paudyal, 2023; Paudyal et al., 2021; Paudyal et al., 2024) in addition to its rugged topography, steep slope and haphazard drainage at and around the river valleys (Dahal and Paudyal, 2022; K.C. et al, 2018).

The differences in influential factors across models can be attributed to the distinct methodologies and assumptions underlying each approach. The FR model is a statistical method that relies on the frequency of landslide occurrences, while the WoE model is based on Bayesian probability theory. The AHP model, on the other hand, is a multi-criteria decision analysis technique that incorporates subjective judgments and expert opinions. All three models agree that slope is a significant factor in landslide susceptibility, with the highest frequency ratio (FR) value of 3.63, WoE of 1.319, and AHP of 0.241 observed in the 50°-60° slope range. Barren land and bush land are identified as significant contributors to landslide susceptibility in all models, with high frequency ratios, WoE values, and AHP weights. The proximity to the thrust (MBT) is a common influential factor, with the 0-500 m distance range being the most prone to landslides in all models. In addition to slope and land-use, the FR model highlights the importance of curvature, with concave slopes having a higher frequency ratio. Distance from the road is also a significant factor, with the 500-1000 m range being the most prone to landslides. The WoE model places more emphasis on the role of geology, with the Gondwana Group having the highest frequency ratio among all geological formations. The WoE model also suggests that the aspect of the slope is a significant factor, with south, southwest, and southeast aspects contributing more to landslides. Each model's strengths and weaknesses are reflected in the factors they emphasize. For instance, the FR model's focus on curvature and distance from the road might be due to its ability to capture spatial relationships and patterns. The WoE model's emphasis on geology and aspect could be attributed to its capacity to handle categorical data and non-linear relationships. The AHP model's consideration of relief, rainfall, and topographic wetness index might be a result of its ability to incorporate expert knowledge and subjective judgments.

Bhandari et al. (2024) conducted several studies in the Siwalik Hills of Nepal using Frequency Ratio (FR), Weights of Evidence (WoE), Information Value (IV), and Shanon Entropy (SE) models to assess landslide susceptibility. Their findings demonstrated the effectiveness of the WoE model with high success (85%) and prediction rates (79.9%). As per the study conducted by Regmi et al. (2014), a success rate of 76.8 % and predictive accuracy of 75.4 % performed better than WoE (success rate, 75.6 %; predictive accuracy, 74.9 %). However in the present study, the Weight of Evidence (WoE) has the highest accuracy (89.9%) in predicting landslides followed by Frequency Ratio (86.4%). While the FR model generally outperformed other models in previous studies, the WOE model showed comparable or even superior results in specific regions, such as the study area. The overall performance of the models varied depending on the study area and specific factors considered. Overall, these studies highlight the importance of carefully selecting and evaluating landslide susceptibility models based on the unique characteristics of each region and the specific research objectives. The resultant susceptibility maps can be useful for general land use planning.

Conclusions

The present study aimed to evaluate the accuracy of three landslide susceptibility assessment methods, namely Frequency Ratio (FR), Analytical Hierarchy Process (AHP), and Weight of Evidence (WoE), in the Ranitar-Belarang section of Udayapur district, Nepal. The causes of landslides are often complex and not fully understood. Through field studies, aerial photography, and geological studies, thirteen factors (geology, slope, aspect, curvature, distance from the stream, distance from the road, distance from the thrust (MBT), relief, land use land cover, rainfall, topographic wetness index, stream power index and sediment transport index) were identified as significant contributors to landslides in the region. These factors were selected based on their relevance, availability, and scale of data. Using the modern GIS technology, it was easier to process large amount of data and prepare landslide susceptibility maps. In this study, the Frequency Ratio model, a statistical method, along with Weight of Evidence, and Analytical Hierarchy Process was employed to assess the spatial probability of landslide occurrence. A total of 120 landslides were identified, with notable influences from factors such as distance from the thrust (MBT), land-use, and slope.

Our results demonstrate the superiority of the WoE method in predicting landslide susceptibility, with a high accuracy of 89.9% compared to FR (86.4%) and AHP (68.5%). This finding is consistent with previous studies that have highlighted the effectiveness of the WoE method in landslide susceptibility assessment. The high ROC/AUC value of 89.9% for the Weight of Evidence method suggests that it performed exceptionally well in predicting landslide susceptibility. This indicates a robust correlation between the input factors and the occurrence of landslides, making the WoE method a reliable and accurate approach for susceptibility mapping.

On the other hand, the Analytical Hierarchy Process exhibited a ROC/AUC value of 68.5%, suggesting a moderate level of accuracy in predicting landslide susceptibility. While not as high as the WoE method, the AHP still demonstrates a meaningful capability to assess landslide-prone areas. And the Frequency Ratio method yielded an ROC/AUC value of 86.4%, indicating a high level of accuracy like the WoE method.

The combination of methods allows for cross-validation, enhancing the overall reliability of the susceptibility map. Therefore, integrating Weight of Evidence, Analytical Hierarchy Process, and Frequency Ratio methods provides a holistic and reliable approach to landslide susceptibility mapping, contributing to more informed decision-making in landslide-prone areas. The landslide susceptibility maps created in this study provide a clear assessment of landslide risk. These maps are valuable resources for citizens, planners, and engineers, aiding in land management and site selection for future development projects. By identifying areas prone to landslides, these maps can help prevent, mitigate, and avoid potential hazards. For instance, areas with high landslide susceptibility can be avoided for development, while areas with low susceptibility can be prioritized for infrastructure development.

References:

Abusarhan, Z. (2011). Application Of Analytic Hierarchy Process (AHP) In The Evaluation and Selection Of an Information System Reengineering Projects. International Journal of Computer Science and Network Security. 11. 172-177.

Acharya, M., Dhakal, R. P., and Paudyal, K. R. (2023). Application of frequency ratio method for landslide susceptibility mapping at the Thulo Lumpek area, Gulmi, Nepal; *Journal of Development Innovations,* © 2022 Karma Quest International, Canada. Link: www.karmaquest.org/journal (ISSN: 2371-9540), vol. 7, No. 2, 56-76.

Aghdam, I. N., Varzandeh, M. H. M., & Pradhan, B. (2016). Landslide susceptibility mapping using an ensemble statistical index (Wi) and adaptive neuro-fuzzy inference system (ANFIS) model at Alborz Mountains (Iran). *Environmental Earth Sciences*, *75*(7), 553. https://doi.org/10.1007/s12665-015-5233-6

Agterberg, F. P., Bonham-Carter, G. F., Cheng, Q. M., & Wright, D. F. (1993). Weights of evidence modeling and weighted logistic regression for mineral potential mapping. *Computers in Geology*, *25*, 13–32.

Althuwaynee, O. F., Pradhan, B., & Lee, S. (2016). A novel integrated model for assessing landslide susceptibility mapping using CHAID and AHP pair-wise comparison. *International Journal of Remote Sensing*, *37*(5), 1190–1209. https://doi.org/10.1080/01431161.2016.1148282

Barbieri, G., & Cambuli, P. (2009). The weight of evidence statistical method in landslide susceptibility mapping of the Rio Pardu Valley (Sardinia, Italy). *In 18th World IMACS Congress and MODSIM09 International Congress on Modelling and Simulation: Interfacing Modelling and Simulation with Mathematical and Computational Sciences, Proceedings*, 2658–2664.

Beven, K. J., & Kirkby, M. J. (1979). A physically based, variable contributing area model of basin hydrology/ Un modèle à base physique de zone d'appel variable de l'hydrologie du bassin versant. Hydrological Sciences Bulletin, 24(1), 43–69. https://doi.org/10.1080/02626667909491834

Bhandari, B. P., Dhakal, S., & Tsou, C.-Y. (2024). Assessing the Prediction Accuracy of Frequency Ratio, Weight of Evidence, Shannon Entropy, and Information Value Methods for Landslide Susceptibility in the Siwalik Hills of Nepal. *Sustainability*, *16*(5), 2092. https://doi.org/10.3390/su16052092

Bonham-Carter, G. F. (1989). Weights of evidence modelling: a new approach to mapping mineral potential. *Statistical Applications in the Earth Sciences*, 171–183.

Bonham-Carter, G. F. (1994). *Geographic Information Systems for Geoscientists*. Elsevier. https://doi.org/10.1016/C2013-0-03864-9

Bonham-Carter, G. F., Agterberg, F. P., & Wright, D. F. (1988). Integration of geological datasets for gold exploration in Nova Scotia. In *Digital Geologic and Geographic Information Systems* (pp. 15–23). American Geophysical Union. https://doi.org/10.1029/SC010p0015

Camarinha, P. I. M., Canavesi, V., & Alvalá, R. C. S. (2014). Shallow landslide prediction and analysis with risk assessment using a spatial model in a coastal region in the state of São Paulo, Brazil. *Natural Hazards and Earth System Sciences*, *14*(9), 2449–2468. https://doi.org/10.5194/nhess-14-2449-2014

Chen, W., Chai, H., Sun, X., Wang, Q., Ding, X., & Hong, H. (2016). A GIS-based comparative study of frequency ratio, statistical index and weights-of-evidence models in landslide susceptibility mapping. *Arabian Journal of Geosciences*, *9*(3), 204. https://doi.org/10.1007/s12517-015-2150-7

Chen, W., Wang, J., Xie, X., Hong, H., Van Trung, N., Bui, D. T., Wang, G., & Li, X. (2016). Spatial prediction of landslide susceptibility using integrated frequency ratio with entropy and support vector machines by different kernel functions. *Environmental Earth Sciences*, *75*(20), 1344. https://doi.org/10.1007/s12665-016-6162-8

Chen, W., Xie, X., Wang, J., Pradhan, B., Hong, H., Bui, D. T., Duan, Z., & Ma, J. (2017). A comparative study of logistic model tree, random forest, and classification and regression tree models for spatial prediction of landslide susceptibility. *CATENA*, *151*, 147–160. https://doi.org/10.1016/j.catena.2016.11.032

Conforti, M., Pascale, S., Robustelli, G., & Sdao, F. (2014). Evaluation of prediction capability of the artificial neural networks for mapping landslide susceptibility in the Turbolo River catchment (northern Calabria, Italy). *CATENA*, *113*, 236–250. https://doi.org/10.1016/j.catena.2013.08.006

Dahal, A., and Paudyal, K.R. (2022). Mapping of Geological Sensitive Areas along the Budhi Khola Watershed, Sunsari/Morang Districts, Eastern Nepal Himalaya. Journal of Development Innovations, © 2022 Karma Quest International, Canada. Link: www.karmaquest.org/journal (ISSN: 2371-9540), Vol. 6, No. 1, 44-68.

Dahal, R. K., Hasegawa, S., Nonomura, A., Yamanaka, M., Masuda, T., & Nishino, K. (2008). GIS-based weights-of-evidence modelling of rainfall-induced landslides in small catchments for landslide susceptibility mapping. *Environmental Geology*, *54*(2), 311–324. https://doi.org/10.1007/s00254-007-0818-3

Dai, F. C., Lee, C. F., Li, J., & Xu, Z. W. (2001). Assessment of landslide susceptibility on the natural terrain of Lantau Island, Hong Kong. *Environmental Geology*, *40*(3), 381–391. https://doi.org/10.1007/s002540000163

Demir, G., Aytekin, M., Akgün, A., İkizler, S. B., & Tatar, O. (2013). A comparison of landslide susceptibility mapping of the eastern part of the North Anatolian Fault Zone (Turkey) by likelihood-frequency ratio and analytic hierarchy process methods. *Natural Hazards*, *65*(3), 1481–1506. https://doi.org/10.1007/s11069-012-0418-8

Ding, Q., Chen, W., & Hong, H. (2017). Application of frequency ratio, weights of evidence and evidential belief function models in landslide susceptibility mapping. *Geocarto International*, 1–21. https://doi.org/10.1080/10106049.2016.1165294

Department of Mines and Geology. (1984). Geological Map of Eastern Nepal. Lainchaur, Kathmandu, (map available in a single sheet).

Ercanoglu, M., Gokceoglu, C., & Van Asch, T. W. J. (2004). Landslide Susceptibility Zoning of North of Yenice (NW Turkey) by Multivariate Statistical Techniques. *Natural Hazards*, *32*(1), 1–23. https://doi.org/10.1023/B:NHAZ.0000026786.85589.4a

Fayez, L., Pazhman, D., Pham, B. T., Dholakia, M. B., Solanki, H. A., Khalid, M., & Prakash, I. (2018). Application of Frequency Ratio Model for the Development of Landslide Susceptibility Mapping at Part of Uttarakhand State, India. *International Journal of Applied Engineering Research*, *13*(9), 6846–6854.

Feizizadeh, B., Shadman Roodposhti, M., Jankowski, P., & Blaschke, T. (2014). A GIS-based extended fuzzy multi-criteria evaluation for landslide susceptibility mapping. *Computers & Geosciences*, *73*, 208–221. https://doi.org/10.1016/j.cageo.2014.08.001

Goetz, J. N., Brenning, A., Petschko, H., & Leopold, P. (2015). Evaluating machine learning and statistical prediction techniques for landslide susceptibility modeling. *Computers & Geosciences*, *81*, 1–11. https://doi.org/10.1016/j.cageo.2015.04.007

Gómez, H., & Kavzoglu, T. (2005). Assessment of shallow landslide susceptibility using artificial neural networks in Jabonosa River Basin, Venezuela. *Engineering Geology*, *78*(1–2), 11–27. https://doi.org/10.1016/j.enggeo.2004.10.004

Greenway, D. . (1987). *Vegetation and slope stability. In: Anderson M.G., Richards, K.S (eds) slope stability*. 187–230.

Hasegawa, S., Nonomura, A., Dahal, R. K., Yuichi, T., Haruki, M., & Yatabe, R. (2008). Geomorphological approach for earthquake-induced landslides study. *International Conference on Disasters and Development*, 94–105.

Hong, H., Pourghasemi, H. R., & Pourtaghi, Z. S. (2016). Landslide susceptibility assessment in Lianhua County (China): A comparison between a random forest data mining technique and bivariate and multivariate statistical models. *Geomorphology*, *259*, 105–118. https://doi.org/10.1016/j.geomorph.2016.02.012

ICIMOD, (2020). Landuse and Landcover Map of Nepal. http://rds.icimod.org/Home/Index

Kamp, U., Growley, B. J., Khattak, G. A., & Owen, L. A. (2008). GIS-based landslide susceptibility mapping for the 2005 Kashmir earthquake region. *Geomorphology*, *101*(4), 631–642. https://doi.org/10.1016/j.geomorph.2008.03.003

Kannan, M., Saranathan, E., & Anabalagan, R. (2013). Landslide vulnerability mapping using frequency ratio model: a geospatial approach in Bodi-Bodimettu Ghat section, Theni district, Tamil Nadu, India. *Arabian Journal of Geosciences*, *6*(8), 2901–2913. https://doi.org/10.1007/s12517-012-0587-5

K. C., J., Gautam, D., Neupane, P., & Paudyal, K. R. (2018). Landslide inventory mapping and assessment along the Ramche-Jharlang area in Dhading, Rasuwa, and Nuwakot districts, Lesser Himalaya, central Nepal. *Journal of Nepal Geological Society, 55*(Sp. Issue), 103-108. https://doi.org/10.3126/jngs.v55i1.22798.

Kemp, L. D., Bonham-Carter, G. F., Raines, G. L., & Looney, C. G. (2001). *Arc-SDM: A review extension for Weight of Evidence Mapping Ottawa, Canada*.

Lee, M.-J., Park, I., & Lee, S. (2015). Forecasting and validation of landslide susceptibility using an integration of frequency ratio and neuro-fuzzy models: a case study of Seorak mountain area in Korea. *Environmental Earth Sciences*, *74*(1), 413–429. https://doi.org/10.1007/s12665-015-4048-9

Lee, M. J., Park, I., Won, J. S., & Lee, S. (2016). Landslide hazard mapping considering rainfall probability in Inje, Korea. *Geomatics, Natural Hazards and Risk*, *7*(1), 424–446. https://doi.org/10.1080/19475705.2014.931307

Lee, S., Hong, S.-M., & Jung, H.-S. (2017). A Support Vector Machine for Landslide Susceptibility Mapping in Gangwon Province, Korea. *Sustainability*, *9*(1), 48. https://doi.org/10.3390/su9010048

Lee, S., & Park, I. (2013). Application of decision tree model for the ground subsidence hazard mapping near abandoned underground coal mines. *Journal of Environmental Management*, *127*, 166–176. https://doi.org/10.1016/j.jenvman.2013.04.010

Lee, S., & Talib, J. A. (2005). Probabilistic landslide susceptibility and factor effect analysis. *Environmental Geology*, *47*(7), 982–990. https://doi.org/10.1007/s00254-005-1228-z

Mondal, S., & Maiti, R. (2013). Integrating the Analytical Hierarchy Process (AHP) and the frequency ratio (FR) model in landslide susceptibility mapping of Shiv-khola watershed, Darjeeling Himalaya. *International Journal of Disaster Risk Science*, *4*(4), 200–212. https://doi.org/10.1007/s13753-013-0021-y

Moore, I. D., & Burch, G. J. (1986). Physical Basis of the Length-slope Factor in the Universal Soil Loss Equation. Soil Science Society of America Journal, 50(5), 1294–1298. https://doi.org/10.2136/sssaj1986.03615995005000050042x

Neupane, A., Paudyal, K. R., Devkota, K. C., & Dhungana, P. (2023). Landslide susceptibility analysis using frequency ratio and weight of evidence approaches along the Lakhandehi Khola watershed in the Sarlahi District, southern Nepal. *Geographical Journal of Nepal*, *16*(01), 73–96. https://doi.org/10.3126/gjn.v 16i01.53486.

Neupane, A., & Paudyal, K. R. (2021). Lithological Control on Landslide in the Siwalik Section of the Lakhandehi Khola Watershed of Sarlahi District, South-Eastern Nepal. Journal of Development Innovations, © 2022 Karma Quest International, Canada. Link: www.karmaquest.org/journal (ISSN: 2371-9540), Vol. 5, No. 2, 44-65.

Park, I., Lee, J., & Saro, L. (2014). Ensemble of ground subsidence hazard maps using fuzzy logic. *Open Geosciences*, *6*(2), 207–218. https://doi.org/10.2478/s13533-012-0175-y

Pathak, D., Maharjan, R., Maharjan, N., Shrestha, S. R., & Timilsina, P. (2021). Evaluation of parameter sensitivity for groundwater potential mapping in the mountainous region of Nepal Himalaya. *Groundwater for Sustainable Development*, *13*, 100562. https://doi.org/10.1016/j.gsd.2021.100562.

Paudyal, K. R., Maharjan, R., and Shrestha, B. (2024). Landslide susceptibility mapping of the main boundary thrust region in Thungsingdanda-Bandipur section of Nawalparasi and Palpa Districts, Gandaki and Lumbini Provinces, Nepal. The Geographical Journal of Nepal. Vol. 17:23-52, DOI: https://doi.org/10.3126/gjn.v17i01.63934

Paudyal, K. R., and Maharjan, R. (2023). Landslide susceptibility mapping of the Main Boundary Thrust region in Mandre-Khursanibari section of Arghakhanchi and Palpa districts, Lumbini province of Nepal. Nepalese Journal of Environmental Science, 11 (2), 35-53; https://doi.org/10.3126/njes.v11i2.58152

Paudyal, K. R., & Maharjan, R. (2022). Landslide susceptibility mapping of the Main Boundary Thrust (MBT) region in Tinau-Mathagadhi Section of Palpa District, Lumbini Province. *Journal of Nepal Geological Society*. *63*, 99–108. *https://doi.org/10.3126/jngs.v63i01.50845.*

Paudyal, K. R., Devkota, K. C., Parajuli, B. P., Shakya, P., & Baskota, P. (2021). Landslide Susceptibility Assessment using open-source data in the far western Nepal Himalaya: A case study from selected local level units. *Journal of Institute of Science and Technology, 26*(2), 31-42 (2021) *ISSN: 2467-9062 (print), e-ISSN: 2467-9240* https://doi.org/10.3126/jist.v26i2.41327.

Peng, L., Niu, R., Huang, B., Wu, X., Zhao, Y., & Ye, R. (2014). Landslide susceptibility mapping based on rough set theory and support vector machines: A case of the Three Gorges area, China. *Geomorphology*, *204*, 287–301. https://doi.org/10.1016/j.geomorph.2013.08.013

Pham, B. T., Tien Bui, D., Dholakia, M. B., Prakash, I., & Pham, H. V. (2016). A Comparative Study of Least Square Support Vector Machines and Multiclass Alternating Decision Trees for Spatial Prediction of Rainfall-Induced Landslides in a Tropical Cyclones Area. *Geotechnical and Geological Engineering*, *34*(6), 1807–1824. https://doi.org/10.1007/s10706-016-9990-0

Pokhrel, K., & Bhandari, B. P. (2019). Identification of Potential Landslide Susceptible Area in the Lesser Himalayan Terrain of Nepal. Journal of Geoscience and Environment Protection, 7, 24-38. https://doi.org/10.4236/gep.2019.711003

Pourghasemi, H. R., Pradhan, B., & Gokceoglu, C. (2012). Application of fuzzy logic and analytical hierarchy process (AHP) to landslide susceptibility mapping at Haraz watershed, Iran. *Natural Hazards*, *63*(2), 965–996. https://doi.org/10.1007/s11069-012-0217-2

Pradhan, B. (2010). Landslide susceptibility mapping of a catchment area using frequency ratio, fuzzy logic and multivariate logistic regression approaches. *Journal of the Indian Society of Remote Sensing*, *38*(2), 301–320. https://doi.org/10.1007/s12524-010-0020-z

Pradhan, B. (2011). Manifestation of an advanced fuzzy logic model coupled with Geo-information techniques to landslide susceptibility mapping and their comparison with logistic regression modelling. *Environmental and Ecological Statistics*, *18*(3), 471–493. https://doi.org/10.1007/s10651-010-0147-7

Pradhan, B. (2013). A comparative study on the predictive ability of the decision tree, support vector machine and neuro-fuzzy models in landslide susceptibility mapping using GIS. *Computers & Geosciences*, *51*, 350–365. https://doi.org/10.1016/j.cageo.2012.08.023

Pradhan, B., & Lee, S. (2010). Landslide susceptibility assessment and factor effect analysis: backpropagation artificial neural networks and their comparison with frequency ratio and bivariate logistic regression modelling. *Environmental Modelling & Software*, *25*(6), 747–759. https://doi.org/10.1016/j.envsoft.2009.10.016

Regmi, A. D., Devkota, K. C., Yoshida, K., Pradhan, B., Pourghasemi, H. R., Kumamoto, T., & Akgun, A. (2014). Application of frequency ratio, statistical index, and weights-of-evidence models and their comparison in landslide susceptibility mapping in Central Nepal Himalaya. *Arabian Journal of Geosciences*, *7*(2), 725–742. https://doi.org/10.1007/s12517-012-0807-z

Regmi, A. D., Dhital, M. R., Zhang, J., Su, L., & Chen, X. (2016). Landslide susceptibility assessment of the region affected by the 25 April 2015 Gorkha earthquake of Nepal. *Journal of Mountain Science*, *13*(11), 1941–1957. https://doi.org/10.1007/s11629-015-3688-2

Regmi, N. R., Giardino, J. R., & Vitek, J. D. (2010). Modeling susceptibility to landslides using the weight of evidence approach: Western Colorado, USA. *Geomorphology*, *115*(1–2), 172–187. https://doi.org/10.1016/j.geomorph.2009.10.002

Reichenbach, P., Busca, C., Mondini, A. C., & Rossi, M. (2014). The Influence of Land Use Change on Landslide Susceptibility Zonation: The Briga Catchment Test Site (Messina, Italy). *Environmental Management*, *54*(6), 1372–1384. https://doi.org/10.1007/s00267-014-0357-0

Reis, S., Yalcin, A., Atasoy, M., Nisanci, R., Bayrak, T., Erduran, M., Sancar, C., & Ekercin, S. (2012). Remote sensing and GIS-based landslide susceptibility mapping using frequency ratio and analytical hierarchy methods in Rize province (NE Turkey). *Environmental Earth Sciences*, *66*(7), 2063–2073. https://doi.org/10.1007/s12665-011-1432-y

Reneau, S., & Dietrich, W. (1987). Size and location of colluvial landslides in a steep forested landscape. *IAHS-AISH Publication*, *165*(165), 39–48.

Saaty, T. (1980). The Analytic Hierarchy Process. *McGraw-Hill, New York*.

Saaty, T. L. (2004). Decision making — the Analytic Hierarchy and Network Processes (AHP/ANP). *Journal of Systems Science and Systems Engineering*, *13*(1), 1–35. https://doi.org/10.1007/s11518-006-0151-5

Shahi, Y. B., Kadel, S., Dangi, H., Adhikari, G., K. C, D., Paudyal, K. R. (2022). Geological Exploration, Landslide Characterization and Susceptibility Mapping at the Boundary between Two Crystalline Bodies in Jajarkot, Nepal. Geotechnics, v. 2(4), pp. 1059-1083.

Steger, S., Brenning, A., Bell, R., Petschko, H., & Glade, T. (2016). Exploring discrepancies between quantitative validation results and the geomorphic plausibility of statistical landslide susceptibility maps. *Geomorphology*, *262*, 8–23. https://doi.org/10.1016/j.geomorph.2016.03.015

Thapa, D., & Bhandari, B. P. (2019). GIS-Based Frequency Ratio Method for Identification of Potential Landslide Susceptible Area in the Siwalik Zone of Chatara-Barahakshetra Section, Nepal. Open Journal of Geology, 09(12), 873–896. https://doi.org/10.4236/ojg.2019.912096

Tien Bui, D., Tuan, T. A., Hoang, N.-D., Thanh, N. Q., Nguyen, D. B., Van Liem, N., & Pradhan, B. (2017). Spatial prediction of rainfall-induced landslides for the Lao Cai area (Vietnam) using a hybrid intelligent approach of least squares support vector machines inference model and artificial bee colony optimization. *Landslides*, *14*(2), 447–458. https://doi.org/10.1007/s10346-016-0711-9

Tsangaratos, P., & Benardos, A. (2014). Estimating landslide susceptibility through a artificial neural network classifier. *Natural Hazards*, *74*(3), 1489–1516. https://doi.org/10.1007/s11069-014-1245-x

Tsangaratos, P., & Ilia, I. (2016). Landslide susceptibility mapping using a modified decision tree classifier in the Xanthi Perfection, Greece. *Landslides*, *13*(2), 305–320. https://doi.org/10.1007/s10346-015-0565-6

Umar, Z., Pradhan, B., Ahmad, A., Jebur, M. N., & Tehrany, M. S. (2014). Earthquake induced landslide susceptibility mapping using an integrated ensemble frequency ratio and logistic regression models in West Sumatera Province, Indonesia. *CATENA*, *118*, 124–135. https://doi.org/10.1016/j.catena.2014.02.005

Van Westen, C. J., Rengers, N., & Soeters, R. (2003). Use of Geomorphological Information in Indirect Landslide Susceptibility Assessment. *Natural Hazards*, *30*(3), 399–419. https://doi.org/10.1023/B:NHAZ.0000007097.42735.9e

Wang, L.-J., Guo, M., Sawada, K., Lin, J., & Zhang, J. (2015). Landslide susceptibility mapping in Mizunami City, Japan: A comparison between logistic regression, bivariate statistical analysis and multivariate adaptive regression spline models. *CATENA*, *135*, 271–282. https://doi.org/10.1016/j.catena.2015.08.007

Wang, Q., & Li, W. (2017). A GIS-based comparative evaluation of analytical hierarchy process and frequency ratio models for landslide susceptibility mapping. *Physical Geography*, *38*(4), 318–337. https://doi.org/10.1080/02723646.2017.1294522

Wilson, J. P., & Gallant, J. C. (2000). Digital terrain analysis. Terrain analysis: Principles and applications, 6(12), 1-27.

William H., (2008). Integrated analytic hierarchy process and its applications – A literature review, European Journal of Operational Research, 86(1), 211-228, ISSN 0377-2217, https://doi.org/10.1016/j.ejor.2007.01.004.

Wu, Y., Li, W., Wang, Q., Liu, Q., Yang, D., Xing, M., Pei, Y., & Yan, S. (2016). Landslide susceptibility assessment using frequency ratio, statistical index and certainty factor models for the Gangu County, China. *Arabian Journal of Geosciences*, *9*(2), 84. https://doi.org/10.1007/s12517-015-2112-0

Yalcin, A., Reis, S., Aydinoglu, A. C., & Yomralioglu, T. (2011). A GIS-based comparative study of frequency ratio, analytical hierarchy process, bivariate statistics and logistics regression methods for landslide susceptibility mapping in Trabzon, NE Turkey. *CATENA*, *85*(3), 274–287. https://doi.org/10.1016/j.catena.2011.01.014

Yilmaz, I. (2009). Landslide susceptibility mapping using frequency ratio, logistic regression, artificial neural networks and their comparison: A case study from Kat landslides (Tokat—Turkey). *Computers & Geosciences*, *35*(6), 1125–1138. https://doi.org/10.1016/j.cageo.2008.08.007